



SIRP α maintains macrophage homeostasis by interacting with PTK2B kinase in *Mycobacterium tuberculosis* infection and through autophagy and necroptosis

Di Wang,^{a,b,d,1} Yunkai Lin,^{a,1} Feihong Xu,^{b,1} Hui Zhang,^c Xiaoyan Zhu,^d Zhen Liu,^d Yuan Hu,^b Guanjun Dong,^c Bingqi Sun,^e Yanhong Yu,^f Guoren Ma,^g Zhigang Tang,^h Diana Legarda,^b Adrian Ting,^b Yuan Liu,ⁱ Jia Hou,^{j***} Liwei Dong,^{a***} and Huabao Xiong^{c*}

^aInternational Cooperation Laboratory on Signal Transduction, Eastern Hepatobiliary Surgery Institute, the Second Military Medical University, Shanghai, National Center for Liver Cancer, Shanghai, China

^bDepartment of Medicine, Precision Immunology Institute, Icahn School of Medicine at Mount Sinai, New York, America

^cInstitute of Immunology and Molecular Medicine, Jining Medical University, Jining Shandong, China

^dThe Eighth Medical Center, Chinese PLA General Hospital, Beijing, China

^eDepartment of Clinical Laboratory, Shenyang Thoracic Hospital, Shenyang Liaoning, China

^fDepartment of Clinical Laboratory, Shenyang Tenth People's Hospital, Shenyang Liaoning, China

^gNingxia No. 4 People's Hospital, Yinchuan Ningxia, China

^hHunan Chest Hospital, Changsha Hunan, China

ⁱProgram of Immunology and Cell Biology, Department of Biology, Center for Diagnostics & Therapeutics, Georgia State University, Atlanta, America

^jDepartment of Respiratory and Critical Care Medicine, General Hospital of Ningxia Medical University, Yinchuan Ningxia, China

Summary

Background To determine whether SIRP α can be a diagnostic marker of pulmonary tuberculosis (PTB) and the molecular mechanism of SIRP α regulating macrophages to kill *Mycobacterium tuberculosis* (MTB).

Methods Meta-analysis combined with subsequent qRT-PCR, western-blotting and flow cytometry assay were used to detect SIRP α expression in PTB patients. Cell-based assays were used to explore the regulation of macrophage function by SIRP α . SIRP $\alpha^{-/-}$ and wide type macrophages transplanted C57BL/6J mice were used to determine the function of SIRP α on MTB infection in vivo.

Findings SIRP α levels are closely correlated with the treatment outcomes among PTB patients. Cell-based assay demonstrated that MTB significantly induces the expression of SIRP α on macrophages. SIRP α deficiency enhances the killing ability of macrophages against MTB through processes that involve enhanced autophagy and reduced necroptosis of macrophages. Mechanistically, SIRP α forms a direct interaction with PTK2B through its intracellular C-terminal domain, thus inhibiting PTK2B activation in macrophages. Necroptosis inhibition due to SIRP α deficiency requires PTK2B activity. The transfer of SIRP α -deficient bone marrow-derived macrophages (BMDMs) into wild type mice resulted in a drop of bacterial load in the lungs but an enhancement of inflammatory lung damage, and the combination of ulinastatin and SIRP $\alpha^{-/-} \rightarrow$ WT treatment could decrease the inflammation and maintain the bactericidal capacity.

Interpretation Our data define SIRP α a novel biomarker for tuberculosis infection and underlying mechanisms for maintaining macrophage homeostasis.

eBioMedicine 2022;85:104278

Published online xxx

<https://doi.org/10.1016/j.ebiom.2022.104278>

ebiom.2022.104278

*Corresponding author at: Institute of Immunology and Molecular Medicine, Jining Medical University, Jining Shandong, China.

**Corresponding author at: International Cooperation Laboratory on Signal Transduction, Eastern Hepatobiliary Surgery Institute, the Second Military Medical University, Shanghai, China.

***Corresponding author at: Department of Respiratory and Critical Care Medicine, General Hospital of Ningxia Medical University, Yinchuan Ningxia, China.

E-mail addresses: houlj@live.com (J. Hou), donliwei@126.com (L. Dong), xionghbl@yahoo.com (H. Xiong).

¹ These three authors contribute equal to this work.

Funding This work was financially supported by the Chinese National Natural Science Foundation project (No.81401635). The funders had no role in study design, data collection and analysis, decision to publish, or preparation of the manuscript.

Copyright © 2022 The Author(s). Published by Elsevier B.V. This is an open access article under the CC BY-NC-ND license (<http://creativecommons.org/licenses/by-nc-nd/4.0/>)

Keywords: Macrophage; Necroptosis; Autophagy; Immune response; Biomarker

Research in context

Evidence before this study

Macrophages serve as the first line of defense against MTB. SIRP α has been reported to negatively regulate the macrophages proinflammatory function.

Added value of this study

We found that SIRP α forms a direct interaction with PTK2B through its intracellular C-terminal domain and compromises the interaction between PTK2B and SHP-1, thus inhibiting PTK2B activation in macrophages. Inhibited PTK2B by SIRP α could decrease autophagy and enhance necroptosis, which play the key role in intracellular tuberculosis clearance.

Implications of all the available evidence

Our findings provide exciting insights into the pathogenesis of tuberculosis and suggest that novel therapeutics that block SIRP α might be beneficial in the management of MTB infection, opening a wealth of new possibilities in the treatment of PTB.

Introduction

Mycobacterium tuberculosis (MTB) is the pathogen responsible for pulmonary tuberculosis (PTB). Anti-MTB treatments are usually long, and the treatment outcomes are uncertain due to increasing MTB resistance; therefore, the global status of PTB is still a global emergency.¹ One of the clinical problems of PTB is that there are few useful indicators to predict disease activity, therapeutic response, relapse, and mortality. In addition, few markers can distinguish PTB from other lung diseases such as pneumonia and lung cancer.²

Microarrays have been widely used to determine the global differentially expressed genes in response to MTB infection in patients.³ Unfortunately, there is only modest overlap in the set of genes identified among the studies, probably as a result of multiple factors such as lab-specific effect, region-, and treatment-specific effects. On this understanding, a meta-analysis of

multiple microarray data would be a powerful tool to define PTB-associated genes. In this study, by performing a meta-analysis on six PTB blood microarray experiments, we identified a series of targets, among which the signal regulatory protein α (SIRP α , also called CD172a), an immunosuppressive factor, was found to be specifically upregulated during MTB infection.

SIRP α is mainly expressed on myeloid cells such as monocytes/macrophages and dendritic cells.⁴ Macrophages act as the first line of defence against MTB by limiting the growth of MTB, and their activity is correlated with MTB clearance.⁵ MTB can also successfully modulate the intracellular environment and thus establish a safe niche within host macrophages for its survival.⁶ Progression of the active PTB disease is almost universally regarded as a ‘failure’ of the host’s immune system to control the infection. This process is usually accompanied by the molecular dysregulation of the critical balance between the macrophages and MTB, which may serve as an instrumental biomarker in determining the outcome of the infection.⁷ Therefore, it is reasonable to assume that the upregulation of the immunosuppressive factor SIRP α in MTB infection could be a means for MTB to escape from macrophage capture. If so, the expression of SIRP α might be closely related to the development and prognosis of PTB.

Many disease markers are also therapeutic targets because they are involved in the regulation of disease progressions. SIRP α is a cell-surface protein, and the cytoplasmic region of SIRP α contains four immunoreceptor tyrosine-based inhibitory motifs (ITIMs) that, upon ligand binding, become phosphorylated and interact with the SH2-domain-containing tyrosine phosphatases (PTPase) SHP-1 and SHP-2 to mediate various biological functions.⁸ Waters et al.⁹ reported that peripheral blood cells expressing SIRP α in *M. bovis*-infected calves proliferated upon in vitro stimulation with ESAT-6/CFP-10, suggesting that SIRP α may have a pivotal role in the immune regulation against MTB. One of the best-documented functions of SIRP α is its inhibitory role in the phagocytosis of host cells by macrophages.¹⁰ van Beek et al.¹¹ demonstrated that SIRP α acts as a critical negative regulator of the respiratory burst, and therefore inhibits the antimicrobial activities of phagocytes against *Salmonella*. Baral et al.¹² also

showed that SIRP α impairs intracellular killing ability against *Burkholderia pseudomallei*. Nevertheless, Li et al.¹³ showed that SIRP α mutant mice have an increased susceptibility to infection with *Salmonella typhimurium*, indicating that SIRP α may also be required for successful host defense against infection. These reports indicate that the role of SIRP α in the host's defence against infection is complicated and should be further explored.

In order to evaluate whether SIRP α is a target of anti-MTB immunotherapy, we explored how SIRP α regulates the interaction between macrophages and MTB. In this report, we demonstrated that high levels of SIRP α predict poor treatment outcomes in patients with PTB. Interestingly, we aimed at first at examining the involvement of SIRP α in autophagy in the context of MTB infection, but the results suggested that SIRP α was also involved in necroptosis. As such, SIRP α negatively regulates PTK2B activity, subsequently inhibiting autophagy and promoting necroptosis. Our findings provide exciting insights into the pathogenesis of tuberculosis and suggest that novel therapeutics that block SIRP α might be beneficial in the management of MTB infection, opening a wealth of new possibilities in the treatment of PTB.

Materials and methods

Ethics

The human study was approved by the Ethics Committee of all involved hospitals (the Eighth Medical Center, Chinese People's Liberation Army (PLA) General Hospital (named PLA 309 hospital before 2018) as the lead site, ethical approval #2014GKJ003). Informed consent was obtained from all patients before participation. All experiments were carried out according to the principles of the Helsinki Declaration.

The animal study protocols were prepared before the study and were registered in and approved by the Institutional Animal Care and Use Committees of the Eighth Medical Center, Chinese PLA General Hospital (ethical approval #2016GKJ009).

Meta-analysis

Gene expression data sets were queried from the GEO database (<https://www.ncbi.nlm.nih.gov/geo/>) using key words such as "tuberculosis" and "human" and using either RNA microarrays or RNA high-throughput sequencing platform. The datasets that included latent tuberculosis infections were excluded. For each dataset, we normalized the gene expression profiles using the quantile method (method="Q") using the IntClust package in R (3.5.1), filtering out genes with >75% missing values. Differentially expressed genes were analyzed using a t-test in the limma package in R (v3.5.1). Multiple hypothesis correction for p values were determined

by using Benjamini and Hochberg method.¹⁴ The statistics and P-values for each gene were obtained in each dataset. The metafor package was used to perform the meta-analysis in six datasets (GSE25534, GSE42832, GSE56153, GSE83456, GSE95563, and GSE107731) that satisfied our criteria. Mixed effect models, Hedges estimator REML and Hunter-Schmidt estimator, were used to evaluate the genes in the six datasets. We used metafor packages (<https://wviechtb.github.io/metafor/>) to compute the β , SE, Z-values, P-values, I², and H² for each gene. The integrated gene expression profiles of the six datasets for significantly differentially expressed genes were clustered and plotted as a heatmap for visualization via the pheatmap and RColorBrewer packages in R (3.5.1).

Patient samples

For the patients who agree to join this study and meet the inclusion criteria of each disease group in the hospital, each patient was assigned a random sequence generated by Excel (version 2013). Then the included patients were selected by random numerical sequence.

To verify the results of the meta-analysis, blood samples from 15 outpatients with PTB, 15 outpatients with NSCLC, and 15 HCs from the Eighth Medical Center, Chinese PLA General Hospital Hospitals were used for qRT-PCR preliminary testing. To further study the expression patterns of SIRP α in the blood of patients with PTB, 74 inpatients with PTB from the Eighth Medical Center, Chinese PLA General Hospital, 35 inpatients with PTB from Shenyang Thoracic Hospital, 40 inpatients with PTB from Ningxia No. 4 People's Hospital, 10 inpatients with PTB from the General Hospital of Ningxia Medical University, 43 inpatients with PTB from the Hunan Chest Hospital, and 90 HCs, were included. To study the differential diagnostic characteristics of SIRP α , 36 inpatients with PTB extra-PTB, 29 inpatients with PTB NSCLC, 23 inpatients with community-acquired PA, and 23 patients with latent tuberculosis at the Eighth Medical Center, Chinese PLA General Hospital were included.

The inclusion criteria of PTB subjects were described as following: 1) Refer to the gold standard of PTB diagnosis, subjects whose sputum culture was positive; or 2) Subjects whose sputum smear was positive, and imaging diagnosis also indicated PTB; or 3) Subjects who have granulomatous histopathology of transbronchial lung biopsy and consistent clinicoradiological findings. Patients younger than 18 years old or with incomplete admission or follow-up data were excluded from this study. All patients received double-blind and standard treatment according to the Chinese tuberculosis treatment guidelines.

Blood and BAL samples were drawn at admission before the start of the anti-MTB drugs. Clinical data, including age, sex, comorbidities, history of PTB,

laboratory data, and results of acid-fast smear, mycobacterial culture, and drug susceptibility test, as well as anti-MTB treatment course and outcomes, were recorded in a standardized case report form. The patients with PTB were followed for at least 6 months after anti-MTB treatment or until death.

Isolation of human monocytes/macrophages from BAL and blood samples

BAL were isolated by adding the erythrocyte lysate buffer. PBMCs were isolated by density gradient centrifugation using Ficoll-Paque (GE Healthcare, Waukesha, WI, USA). For those that needed to be stimulated differentiation into macrophages, the cells were cultured in 6-well tissue culture plates (Corning Inc., Corning, NY, USA) at a density of 2×10^6 cells/ml for 7 days in RPMI 1640 medium supplemented with recombinant GM-CSF (10 ng/ml).

Immunohistochemistry of lung tissues

The tissue sections (3- μ m thick) were dewaxed, rehydrated, and immersed in methanol containing 0.3% hydrogen peroxide (Sinopharm Chemical Reagent Co., Ltd., Beijing, China, #10011218) for 30 min to block endogenous peroxidase activity. The sections were heated in a pressure cooker filled with 10 mM ethylenediaminetetraacetic (EDTA, Sigma, St Louis, MO, USA, #34550) buffer (pH 8.0) for 2 min. After cooling, the sections were incubated in 1% blocking serum (Chemicon, Temecula, CA, USA, #20773) for 30 min to reduce nonspecific binding. Primary SIRP α (Cell Signaling Technology, Danvers, MA, USA, #13379) or PTK2B phosphorylation (Invitrogen Inc., Carlsbad, CA, USA, #44-618G) antibodies were diluted 1:350 and incubated with the sections at 4°C overnight. Sections without antibody incubation were set as negative control. Following incubation with biotinylated secondary antibody (Millipore Corp., Billerica, MA, USA, #20775), the streptavidin-biotin complex/horseradish peroxidase (Millipore Corp., Billerica, MA, USA, #20774) was added. Finally, the signal was developed with diaminobenzidine (Dako, Glostrup, Denmark, #K3468), and the slides were counterstained in haematoxylin. Stained sections were quantified in a blinded manner without prior knowledge of the clinical information using the German immunoreactive score (IRS). IRS was calculated by multiplying the intensity of stain (0-4) with the percentage of positive cells (0-4) and scores ranging from 0 to 16 were obtained. IRS over 8 was considered as "high level", and IRS within 0-8 was considered as "low level".

Strains and colony-forming unit (CFU) determination

The Bacille Calmette Guerin (BCG) and standard MTB H37Rv strains (ATCC 27294) were purchased from the Beijing Institute for Tuberculosis Control. Ten clinical

isolates, which were identified and characterized for their susceptibility to the first line and second-line antibiotics by our team at the Eighth Medical Center, Chinese PLA General Hospital in our previous work,¹⁴ were randomly selected in this work and numbered from A to J (Supplementary Figure S4a). All isolates were cultured using the Middlebrook 7H10 agar medium before use. *L. monocytogenes* was from the National Center for Medical Culture Collections and was grown on BHI agar plates. *E. coli* was from the National Center for clinical laboratories and was cultured using LB agar medium. For the CFU determination, tissues or cultured cells were homogenized, and the viable bacteria were grown on the appropriate medium and enumerated by the pour plate method after serial dilution. Colonies of *L. monocytogenes* were enumerated 24 h after incubation at 37°C. Colonies of BCG were determined 21 days after incubation at 36.5°C.

Mice

SIRP $\alpha^{-/-}$ mice were constructed and generated in previous reports.¹⁰ RIPK1^(-/-) and RIPK3^(-/-) mice were obtained from Jackson Laboratory (West Grove, PA, USA). Wide type C57BL/6J mice were purchased from Vital River Laboratory Animal Technology Co. Ltd., Beijing, China. All mice were raised at 21-23°C and 40 ~ 60% humidity.

Mice BMDMs preparation

Bone marrow cells were isolated from the tibias and femurs of the mice, and the cells were cultured in a complete DMEM medium supplemented with GM-CSF (10 ng/ml). On day 6 or 7, BMDMs were harvested and seeded in fresh complete DMEM medium at 2×10^6 cells/ml.

Human macrophages culture and sorting

Peripheral blood mononuclear cells (PBMC) were isolated by density gradient centrifugation and macrophages were prepared using published protocols (Specific lipid mediator signatures of human phagocytes: microparticles stimulate macrophage efferocytosis and pro-resolving mediators). Briefly, monocytes were purified using monocyte isolation kit (StemCell Technologies) yielding a 93%-97% CD14⁺ population. These cells were then cultured in tissue culture plates for 7 days in RPMI 1640 (10% human serum). Macrophages were differentiated using 20 ng/mL GM-CSF for 6 or 7 days. Subsequently, cells were harvested and sorted into SIRP α^{high} (CD172a⁺) and SIRP α^{low} (CD172a⁻) subset cells using a FACS-Aria (Becton Dickinson, >98% purity) according to previous report.⁹

Cell line culture

Human embryonic kidney (HEK) 293T cells were provided by Hunan Fenghui Biotechnology Co., Ltd (STR profiling was shown in supplementary file), and were cultured in DMEM (Hyclone, Logan, UT) supplemented with 10% fetal bovine serum (FBS) (Hyclone), 100 units/ml penicillin, 100 mg/ml streptomycin (Invitrogen, Carlsbad, CA, USA) and maintain in 5% CO₂ at 37°C.

Measuring the phagocytosis and killing activity of macrophages on the strains

Measuring the phagocytosis and killing activity of macrophages on the strains was performed according to previous report.¹⁵ Briefly, BMDMs from mice or PBMCs from humans were induced into macrophages by appropriate methods. Subsequently, strains were added to the macrophage cells at MOI (bacteria/cell ratio) of 1:10 and incubated for 2 h at 37°C. Using DMEM medium, cells were washed and fresh DMEM supplemented with 200 µg/ml amikacin was added to the cells further for 2 hours to kill extracellular bacilli. After this four-hour phagocytosis period, infected macrophages were washed with PBS and lysed using 0.05% Tween 20 to release internalized bacteria, and the phagocytosis was measured by CFU counting determination of these bacteria. In rest of the wells, amikacin was removed from medium, and infected cells were further incubated for another 24 h. After completion of 24 h, extracellular bacteria were evaluated by CFU counting determination of culture supernatants, and total mycobacterial number (intracellular and extracellular) was assessed by CFU counting determination of whole cell cultures that were lysed according to previous report.¹⁶ Due to differences in initial phagocytosis of bacteria between groups, the total survival of bacteria is presented as fold change in CFU compared to the initially internalized bacteria.

In vivo PTB modelling and tumour bearing modelling

The 6-8-week-old female C57BL/6J mice, about 20g weight, were pre-numbered, and were randomly divided into three groups, based on the random sequence generated by Excel (version 2013): PTB modelling group; tumour bearing modelling group and healthy control group. For the PTB modelling group, 4-6-week-old female C57BL/6J mice were infected by a transtracheal injection using 0.2 mL of a suspension containing 1×10^3 CFUs of viable BCG or H37Rv cells. The left lung lobes and spleen were removed aseptically on day 28 to identify if the infection was successful. For tumour bearing model, C57BL/6 mice were subcutaneously inoculated with 0.2 ml/each of Lewis cells (1×10^7 cells/ml) below the right forelimb armpit. After 2 weeks, the tumour bearing model was established when the size of the tumour grew to about 65 mm³.

Mice receiving equal volume PBS injection were set as the control group. Each treatment group was composed of eight mice, which were kept in a cage. This sample size was determined on the basis of empirical data from pilot or previous experiments, which were sufficient to detect differences as small as 10% using the statistical methods described. Totally 24 mice were used for this experiment. All mice after specific treatment were tested accordingly.

Macrophage transplantation

The 6-8-week-old female C57BL/6J mice, about 20g weight, were pre-numbered, and were randomly divided into several groups, according to different treatment. Mice were first infected by a transtracheal injection of 0.2 mL of a suspension containing 1×10^3 viable BCG or H37Rv cells, and that receiving equal volume PBS injection were set as the control group. Seven days later, the BCG infected mice, H37Rv infected mice and control mice were injected with GdCl₃ (Sigma, St Louis, MO, USA; 10 mg/kg) to eliminate macrophages *in vivo* and received an injection of 10^7 SIRPα^{-/-} macrophages and the WT controls, together with or without ulinastatin treatment. After 21 days, the mice were sacrificed by CO₂ inhalation, to reduce pain, suffering and distress. The left lung lobes were removed aseptically, homogenized, and plated on Middlebrook 7H10 agar medium (supplemented with oleic acid, albumin, dextrose, and catalase) with 10-fold serial dilutions to determine the CFUs. Samples of right lungs were fixed in 10% formalin and embedded in paraffin, and sections were cut and stained with hematoxylin and eosin or Ziehl-Neelsen acid-fast stain for evaluation of tissue pathologic changes or bacillary load in a blinded fashion by a pathologist. Each treatment group was composed of eight mice, which were kept in a cage. This sample size was determined on the basis of empirical data from pilot or previous experiments, which were sufficient to detect differences as small as 10% using the statistical methods described. Totally 96 mice were used for this experiment. All mice after specific treatment were tested accordingly.

RNA sequencing and analysis

RNA was isolated from about 10^6 cells with TRIZOL reagent (Invitrogen Inc., Carlsbad, CA, USA). Total RNA was purified by the Qiagen RNeasy mini kit (Qiagen, Venlo, The Netherlands, #74106). Purified RNA was analyzed on an ND-8000 spectrophotometer (Nanodrop Technologies, Wilmington, DE, USA), agarose electrophoresis, or a 2100-Bioanalyzer (Agilent Technologies, Santa Clara, CA, USA) to determine the quantity of RNA. Single- and double-stranded cDNA was synthesized from mRNA samples using SuperScript II (Invitrogen Inc., Carlsbad, CA, USA). High

quality total RNA (1 µg) was used as the starting material. The Truseq RNA sample preparation kit (Illumina, Inc., San Diego, CA, USA, #RS-200-0048) was used for mRNA purification and fragmentation, first-strand cDNA synthesis, and second-strand cDNA synthesis. The double strands cDNA was purified for end-repair, dA tailing, adaptor ligation, and DNA fragments enrichment. Quantification of the libraries was done using Qubit (Invitrogen Inc., Carlsbad, CA, USA, #Q33327) according to the Qubit user Guide. The constructed library was sequenced on a HiSeq 4000 sequencer (Illumina, Inc., San Diego, CA, USA).

Read alignment and transcript assembly

The paired-end raw reads were aligned using TopHat version 1.2.0, which allows two mismatches in the alignment. The aligned reads were assembled into transcripts using cufflinks 2.0.0. The alignment quality and distribution of the reads were estimated using SAMtools. From the aligned reads, the de novo transcript assemblies were performed to capture the major splice rearrangements and novel variations that occur in the transcriptomes samples using cufflinks version 1.3.036. The cuffcompare program was used to identify transcripts that were identical to the reference human genome (the Ensembl GRCh37.62 B (hg19) reference genome). Further analysis and novel isoform calls were performed through the reconstructed transfrags that comprise novel splice junctions and share at least one splice junction with a reference transcript. The global statistics, which include the distributions of FPKM scores across samples and the dendrogram that shows the relationship between the samples based on the reconstructed transcripts, were analyzed using the cummeRbund package of the cufflinks suite.

GO and pathway analysis

To associate cellular functions with the set of differential expressed genes, we used Database for Annotation, Visualization and Integrated Discovery (DAVID <http://david.abcc.ncifcrf.gov/>) and Reactome pathway analysis (<https://reactome.org/>).

Cytotrap yeast two-hybrid analysis

Total RNA was isolated from K562 cells (American Type Culture Collection (ATCC), Manassas, VA, USA) using the RNAaqueous kit (Ambion, Thermo Fisher Scientific, Waltham, MA, USA, #AM1920) according to the manufacturer's instructions. Total RNA (200 µg) was obtained, and poly(A) RNA was purified using the Poly (A) Purist kit (Ambion, Thermo Fisher Scientific, Waltham, MA, USA, ##AM1922) according to the manufacturer's instructions. A total of 5 µg of poly(A) RNA was recovered, and a cDNA library was synthesized and cloned into a pMyr XR vector using the Cytotrap XR

library construction kit (Stratagene, Wilmington, DE, USA, #ST200444). The control plasmids for the two-hybrid assay were provided with the kit. The bait plasmid pSOS-HA-NUP98-HOXA9 (pSOS-SIRP α) was constructed by subcloning HA-tagged NUP98-HOXA9 (SIRP α) in-frame from pcDNA3-HA-NUP98-HOXA9. The Cytotrap yeast two-hybrid analysis was performed according to the manufacturer's instructions. Briefly, the mouse lung cDNA library in the pMyr vector and pSOS-HA-NUP98-HOXA9 (pSOS-SIRP α) were co-transformed into the cdc25H yeast strain, plated in a selective medium containing glucose as the carbon source, and incubated at room temperature until the colonies appeared. Colonies were replicated into a selective medium containing galactose as the carbon source and incubated at 37°C until the colonies appeared. Temperature-resistant colonies were isolated, patched into fresh selective plates, grown, and replica-plated again to confirm the growth and eliminate false positives. The patches were grown in a liquid medium to isolate the pMyr plasmid DNA containing the positive clones. The isolated plasmids were amplified in *Escherichia coli*, and purified DNA was sequenced using primers on both sides of the cDNA insert regions. The cDNA inserts were identified using the National Center for Biotechnology Information BLAST application.

Flow cytometry

For flow cytometry analysis of cell-surface markers, the cells were stained with antibodies in PBS containing 0.1% (wt/vol) BSA and 0.1% NaN₃. Human BD Fc block antibody (BD Biosciences Cat# 564219, RRID: AB_2728082) and purified rat anti-mouse CD16/CD32 (Mouse BD Fc Block™) (BD Biosciences Cat# 553141, RRID:AB_394656) were used to block Fc in human samples and mice samples, respectively. Flow cytometry data were acquired on a FACSCalibur (BD Biosciences, Franklin Lake, NJ, USA) or a Beckman Coulter Epics XL benchtop flow cytometer (Beckman Coulter, Brea, CA, USA), and data were analyzed with the FlowJo Software (TreeStar, Ashland, OR, USA). For each batch of SIRP α levels determination, flow cytometry was performed on each tested samples and an additional blank control (cell-free control). The mean fluorescence intensity is considered to represent the SIRP α levels. One healthy control sample (one of the healthy controls) was randomly selected to be tested in each batch. The SIRP α level of this healthy control sample was identified as "1", and the normalized SIRP α levels of all other samples was set as the "fold change" relative to that of control sample. The APC linked CD172a (SIRP α) monoclonal antibody (15-414) (Thermo Fisher Scientific Cat# 17-1729-42, RRID:AB_1944409), the PE linked CD14 monoclonal antibody (61D3) (Thermo Fisher Scientific Cat# 12-0149-42, RRID:AB_10598367) and the PE linked F4/80 monoclonal antibody (BM8) (Thermo

Fisher Scientific Cat# 12-4801-82, RRID:AB_465923) for flow cytometry were all purchased from eBioscience, Thermo Fisher Scientific.

Quantitative RT-PCR assay

RNA was extracted with an RNeasy kit (Qiagen, Venlo, The Netherlands, #74106), and cDNA was synthesized using SuperScript III RT (Invitrogen, Carlsbad, CA, USA). An ABI 7900 real-time PCR system was used for quantitative PCR, with primer and probe sets obtained from Applied Biosystems (Foster City, CA, USA). The results were analyzed using the SDS 2.1 software. The expression of each target gene was presented as the “fold change” relative to that of control samples.

Western blot

The cells were washed with ice-cold phosphate-buffered saline (PBS) and lysed with protein lysate (Pierce, Rockford, IL, USA). After centrifugation at $5000 \times g$ for 15 min at 4°C, the protein concentration was measured with a bicinchoninic acid (BCA) protein assay kit (Pierce Chemical, Dallas, TX, USA). Fifty microgram aliquots of lysates were loaded on a sodium dodecylsulfate (SDS) polyacrylamide 10% gradient gel and transferred to a polyvinylidene difluoride membrane. The membranes were blocked with 5% non-fat dry milk in Tris-buffered saline, pH 7.4, containing 0.05% Tween 20, and were incubated with primary antibodies (1:200; Santa Cruz Biotechnology, Santa Cruz, CA, USA) and horseradish peroxidase-conjugated secondary antibodies (1:5000; Santa Cruz Biotechnology, Santa Cruz, CA, USA) in accordance with manufacturer's instructions. The protein of interest was visualized using enhanced chemiluminescence (ECL) western blotting substrate (Pierce Chemical, Dallas, TX, USA) and the Chemidoc XRS Gel Documentation System (Bio-Rad, Hercules, CA, USA). The primary antibodies used in this study are as follows: CYLD (Cell Signaling Technology Cat# 8462, RRID: AB_10949157); β -actin (Cell Signaling Technology Cat# 3700, RRID: AB_2242334); MLKL (Cell Signaling Technology Cat# 37705, RRID: AB_2799118); p-MLKL (Cell Signaling Technology Cat# 37333, RRID: AB_2799112); SIRP α for western (Cell Signaling Technology Cat# 13379, RRID: AB_2798196); SIRP α for IP: (Santa Cruz Biotechnology Cat# sc-136067, RRID: AB_2188059); iNOS (Cell Signaling Technology Cat# 13120, RRID: AB_2687529); SQSTM1 (Cell Signaling Technology Cat# 39749, RRID: AB_2799160); LC3-I/II (Cell Signaling Technology Cat# 12741, RRID: AB_2617131); PTK2B (Cell Signaling Technology Cat# 3292, RRID: AB_2174097); p-PTK2B (Cell Signaling Technology Cat# 3291, RRID: AB_2300530); UB (Cell Signaling Technology Cat# 3936, RRID: AB_331292); GAPDH (Cell Signaling Technology Cat# 5174, RRID: AB_10622025); FLAG (Abcam Cat# ab125243, RRID:

AB_11001232); Myc (Abcam Cat# ab32, RRID: AB_303599); RIPK1 (Cell Signaling Technology Cat# 3493, RRID: AB_2305314); p-RIPK1 (Cell Signaling Technology Cat# 83613, RRID: AB_2800023).

Cytokine ELISA assay

The supernatants from the cell cultures were collected after activation under various conditions, and the secreted cytokines in the supernatants were measured by ELISA kits. The ELISA kits for IL-12p40 (#PM1240 for mouse and #PD2300B for human), IL-6 (#PM6000B for mouse and PD6050 for human), and TNF α (#PMTA00B for mouse and PDTA00D for human) were purchased from R&D Systems (Minneapolis, MN, USA).

Confocal microscopy

Confocal microscopy was performed as described previously.¹⁷ After the appropriate treatments, the cells on coverslips were washed three times with fresh PBS, fixed with 4% paraformaldehyde for 15 min, permeabilized with 0.25% Triton X-100 (Sigma, St Louis, MO, USA) for 10 min, and incubated with LC3 antibodies (Cell Signaling Technology, Danvers, MA, USA, #4108) or LAMP1 antibodies (Cell Signaling Technology Cat# 3243, RRID: AB_2134478) for 2 h at room temperature. The cells were washed with PBS to remove excess primary antibodies and incubated with secondary antibodies for 1 h at room temperature. Nuclei were stained with DAPI for 1 min. After mounting, fluorescence images were acquired using a confocal laser-scanning microscope (Zeiss 780; Carl Zeiss GmbH, Oberkochen, Germany).

Cell death assay

Cell death was analyzed by propidium iodide staining, followed by flow cytometry. The cells were fixed in cold 70% ethanol for at least 30 min at 4°C. The cells were centrifuged at 2000 rpm for 10 min and resuspended in PBS. The cells were treated with RNase and stained with propidium iodide (Thermo Fisher Scientific, Waltham, MA, USA, #BMS500PI), according to the manufacturer's instructions. The cells were analyzed using a FACSCalibur system (BD Biosciences, Franklin Lake, NJ, USA).

Statistical analysis

We calculated sample size requirement by using PASS software. For clinical sample size determination, COX Regression procedure was used and the parameters were described as following: Power=0.8; Alpha=0.05; P (Overall Event Rate)=0.2; B (Log Hazard Ratio)=1; R-Squared of X_1 with other X 's=0.18; S (Standard Deviation of X_1)=0.571. For mice sample size determination,

Two-Sample T-Tests Assuming Equal Variance procedure was used and the parameters were described as following: Power=0.9; Alpha = 0.05; Group Allocation: $N_1 = N_2$; $\mu_1 = 5.5$; $\mu_2 = 3.8$; $\sigma = 0.98$. All statistical analyses were performed using SPSS 24.0 software (SPSS) and GraphPad (Prism 8.0, GraphPad). Descriptive data were summarized as mean (SD). The difference between two group were compared using Student's t-test for continuous variables and using Pearson's Chi-square test for discrete variables. If any continuous variables were non-parametric, Mann-Whitney U-test was employed. Univariate survival analysis was performed by Kaplan-Meier analysis followed by Log Rank testing. The univariate and Multivariate COX proportional hazards regression analysis was used to evaluate the relationship between the gene expression values and the OS of PTB patients. $P < 0.05$ was considered statistically significant.

Role of funding source

Funders did not participate in study design, data collection, data analyses, interpretation, or writing of report.

Results

Identification of a set of dysregulated genes in PTB using microarray meta-analysis

By searching the gene expression omnibus (GEO) database, we found that six microarray datasets determined the differential transcriptomes in whole blood samples between patients with PTB and healthy controls (Supplementary Table 1). The raw data were extracted from the website database (<https://www.ncbi.nlm.nih.gov/bioproject/>) and were used for the meta-analysis study (Supplementary Dataset 1). A cutoff of meta-P-values at $1E-05$ was used to filter the differentially regulated transcripts, and a total of 76 targets were identified (Figure 1a upper panel). The KEGG pathway enrichment was performed for the 76 identified targets, and the results indicated that 19 targets were immune system-related genes (ISRGs) (Figure 1a below panel). The re-clustered heatmap plot and forest maps of these ISRGs are shown in Figure 1b and Supplementary Figure S1, respectively.

Next, we validated whether the above ISRGs could be the potential PTB specific biomarkers. Considering that the imaging characteristics and many molecular characteristics between non-small cell lung carcinomas (NSCLC) and PTB patients are usually very similar, which makes it difficult to distinguish PTB from NSCLC, we also compared the ISRGs expression profiles in PTB and NSCLC samples. qRT-PCR was used to test the ISRGs' mRNA expression in blood samples from 15 outpatients with PTB, 15 outpatients with NSCLC, and 15 healthy controls at the Eighth Medical

Center, Chinese PLA General Hospital. We found that although the ISRGs' mRNA expressions were mostly higher in PTB patients than in the healthy controls, only SIRP α mRNA expression could differentiate PTB from NSCLC (Figure 1c, $P < 0.05$ for all, MX2, CD74 and NCKAP1L Mann-Whitney U-test, others student t-test). Therefore, we selected SIRP α to determine its protein expression patterns in the clinical samples of patients with PTB from multiple hospitals.

Identification of elevated SIRP α levels in monocytes/macrophages of patients with PTB by multicenter clinical sample testing

The multicenter study was conducted at five hospitals, one in China's capital (Beijing), one in Northeast China (Shenyang), one in Central China (Changsha), and two in Northwest China (Ningxia). The clinical characteristics of the included subjects are shown in Supplementary Table 2. There were no significant differences between patients with PTB and healthy controls regarding age, sex, and body mass index (BMI). Peripheral blood mononuclear cells (PBMCs) and bronchoalveolar lavage leukocytes (BALs) samples were collected from all subjects, and western blotting analysis demonstrated that the SIRP α protein expression was significantly higher in both PBMCs ($P = 0.0244$, student t-test) and BALs ($P = 0.0101$, student t-test) of patients with PTB (Figure 1d). Flow cytometry demonstrated that the monocytes/macrophages of both PBMCs ($P < 0.001$, student t-test) samples and BALs ($P < 0.001$, student t-test) samples (Figure 1e, Supplementary Figure S2) from the patients with PTB also had significantly higher SIRP α levels.

Furthermore, we found that SIRP α expression in blood monocytes/macrophages could distinguish active PTB from latent MTB ($P = 0.0184$, student t-test), NSCLC ($P < 0.001$, student t-test), and infectious pneumonia (PA) subjects ($P = 0.0394$, student t-test), but the differences between PTB patients and extrapulmonary tuberculosis patients ($P = 0.1486$, Mann-Whitney U-test) did not reach statistical significance (Figure 1f).

We then determined the predictive value of SIRP α expressions on PTB prognosis. We assigned the 203 PTB patients to the high SIRP α expression group (SIRP α -H group) and low SIRP α expression group (SIRP α -L group) based on the blood flow cytometry results for monocytes/macrophages and using the median expression of SIRP α as the cutoff value (normalized SIRP α median = 1.48). SIRP α expression could predict 6-month mortality (Figure 1g, $P < 0.001$, Kaplan-Meier). Furthermore, during the initial 2 months of anti-MTB treatments, the sputum smear conversion rate ($P < 0.001$, Kaplan-Meier) and cough conversion rate ($P < 0.001$, Kaplan-Meier) were significantly lower in the SIRP α -high group than in SIRP α -low patients (Figure 1h). Moreover, SIRP α expression positively

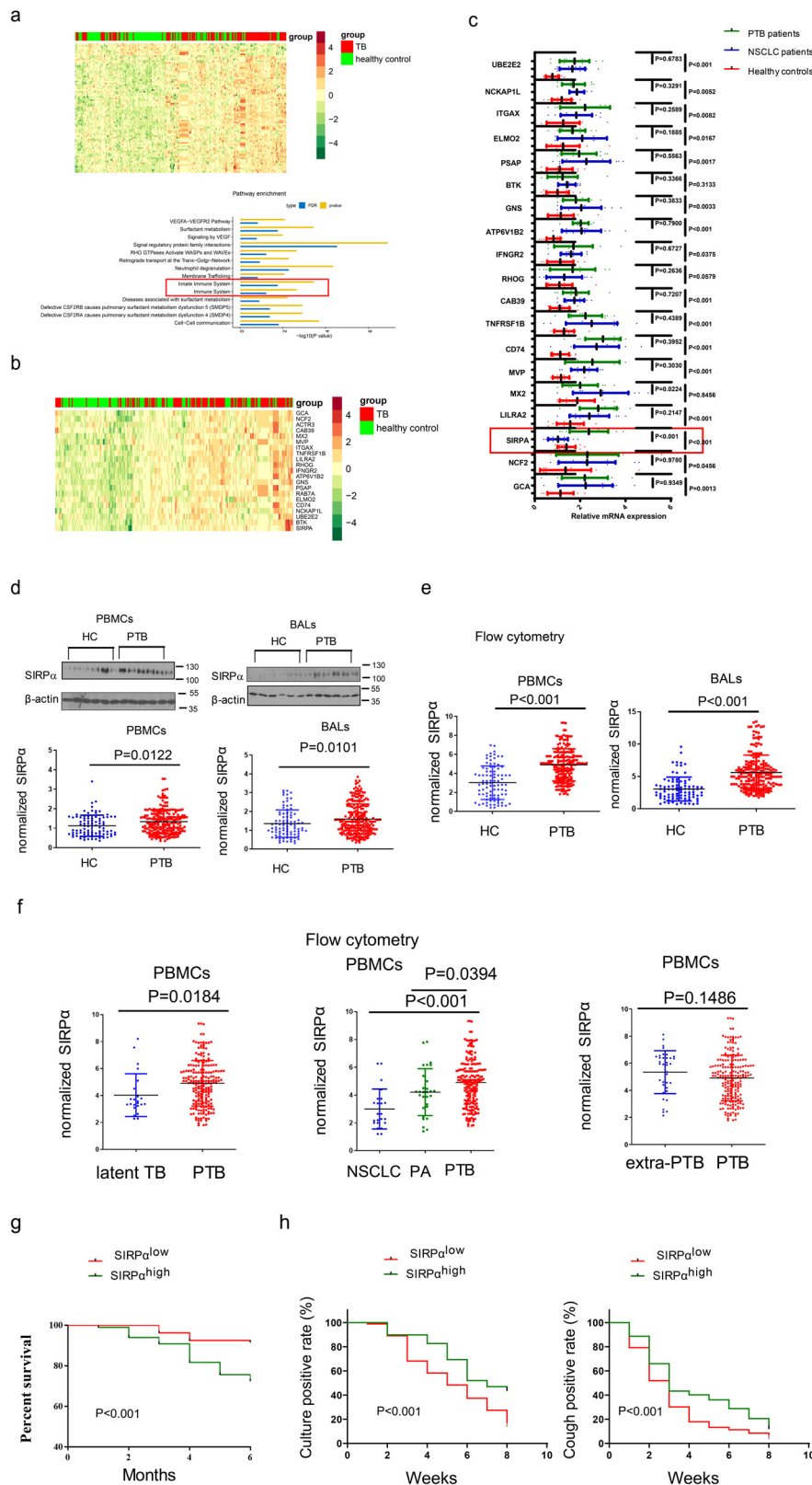


Figure 1. Expansion of SIRP α in patients with PTB compared with HCs. (a) Hierarchical clustering of transcripts expression profiles of the meta-analysis from the six used microarrays (Upper panel). Clustering of all the transcripts in HC and PTB samples. The numbers below the image refer to the various experimental regimens described in Supplementary Table 1. KEGG pathway

correlated with blood disseminated tuberculosis and cigarette use (Supplementary Table 3). These data indicated that high SIRP α expression was correlated with poor treatment outcomes among patients with PTB. To exclude the influence of therapeutic techniques on treatment outcomes, we allocated the patients with PTB according to the hospitals they were visiting. Expectedly, there were no significant differences in the treatment outcomes among hospitals (data not shown). Finally, to determine the prognostic value of SIRP α with regards to outcome, we performed Cox proportion-hazard regression analyses. The univariable analyses demonstrated that several factors, including SIRP α expression, were significant predictors of mortality (Supplementary Table 4). As SIRP α showed association with blood-disseminated tuberculosis and a history of cigarette smoking, a multivariable analysis was performed to assess the independence of the prognostic effect of SIRP α . The results showed that SIRP α , together with blood disseminated tuberculosis pattern, acid-fast staining grade before treatment, and cough grade before treatment, was strongly associated with 6-month mortality (Supplementary Table 5).

Collectively, the above clinical data suggested that SIRP α expression in PBMCs and BALs might have a close relationship with PTB and might be an indicator to distinguish it from other diseases, but the mechanisms involved require additional exploration.

Induced SIRP α expression by MTB suppresses the macrophage phagocytosis and killing abilities against MTB

Therefore, we next used BCG- ($P < 0.001$ for BAL and $P = 0.0017$ for PBMCs, student t-test) and H37Rv- ($P < 0.001$ for BAL and $P < 0.001$ for PBMCs, student t-test) infected mice to explore the effects of MTB on SIRP α expression. Both BCG- and H37Rv-infected mice showed increased SIRP α expression in PBMCs and BALs, while the SIRP α expression in lung cancer mice

($P = 0.037$ for BAL and $P = 0.0061$ for PBMCs) was significantly lower than that of the healthy control group (Supplementary Figure S3a-b). The mouse model results confirmed the clinical findings and prompted us to investigate whether SIRP α could regulate the anti-MTB immunity of macrophages.

Hence, we cultured the PBMCs from three random HC blood each batch, with GM-CSF to promote differentiation into macrophages (marker: CD14⁺), and sorted the cells into CD14⁺SIRP α ^{high} and CD14⁺SIRP α ^{low} subset. SIRP α expressions in these two subsets were confirmed by western blotting assay (data not shown), and these two subsets were cultured again, with BCG or H37Rv challenge at MOI of 10. The phagocytosis ($P = 0.0389$ for BCG and $P = 0.0462$ for H37Rv) and killing ability ($P = 0.0444$ for BCG and $P = 0.0209$ for H37Rv, student t-test) against BCG or H37Rv of SIRP α ^{low} macrophages was stronger than that of the SIRP α ^{high} group (Figure 2a-b). Meanwhile, the pro-inflammatory cytokines, such as COX2 ($P = 0.0311$ for BCG and $P = 0.0367$ for H37Rv), IL-6 ($P = 0.0100$ for BCG and $P = 0.0066$ for H37Rv, student t-test), and TNF α ($P = 0.0286$ for BCG and $P = 0.0255$ for H37Rv, student t-test) in BCG- or H37Rv-stimulated SIRP α ^{low} macrophages were significantly higher than those of SIRP α ^{high} macrophages (Figure 2c). Subsequently, we used SIRP α ^{-/-} and wild type mouse bone marrow-derived macrophages (BMDMs) to generate macrophages, and obtained similar results to those of human macrophages, which all indicated that SIRP α plays a negative regulatory role in macrophage phagocytosis and killing ability against MTB. (Figure 2d-f, $P < 0.05$ for all, student t-test).

We used 10 clinical MTB strains (strains A-J, Supplementary Figure S4a), including multidrug-resistant strains and extensively drug-resistant strains, to challenge the macrophages, and found that the phagocytosis and killing ability of macrophages was similar among different strains (Supplementary Figure S4b-e, $P < 0.05$ for all, student t-test). And, this function was also seen

enrichment for the identified differential targets from the meta-analysis (Lower panel). The red boxes indicate the immune system process-related genes. (b) Clustering of all the immune system process-related genes in HC and PTB samples. (c) qRT-PCR assay showing the differential expressing patterns of the genes described in (b) among 15 PTB patients, 15 NSCLC patients, and 15 HCs (MX2, CD74 and NCKAP1L Mann-Whitney U-test, others student t-test). (d) Western-blotting assay showing the expansion of SIRP α in PBMCs samples (student t-test) and BALs samples (Mann-Whitney U-test) between 203 PTB patients and 90 HCs. (e) Flow cytometry assay showing the expansion of SIRP α in CD14⁺ monocytes/macrophages obtained from PBMCs (student t-test) and BALs (student t-test) samples between 203 PTB patients and 90 HCs. (f) Flow cytometry assay showing SIRP α expression of blood CD14⁺ monocytes/macrophages were higher in active PTB patients ($n = 203$) than in latent TB ($n = 23$) cases (left panel, student t-test) and NSCLC ($n = 29$) and PA ($n = 23$) patients (middle panel, student t-test), but not significantly different with extra-PTB ($n = 36$) patients (right panel, Mann-Whitney U-test). (g-h) The 203 PTB inpatients were followed regularly over the next six months, and their (g) survival curves and (h) culture-positive curves and cough-positive curves were plotted using the Kaplan-Meier method. Red curve: H group; Blue curve: L group.

PTB: pulmonary tuberculosis; HCs: healthy controls; NSCLC: non-small cell lung cancer; PA: pneumonia; extra-PTB: extrapulmonary tuberculosis.

Results are shown as means \pm SD of three experiments.

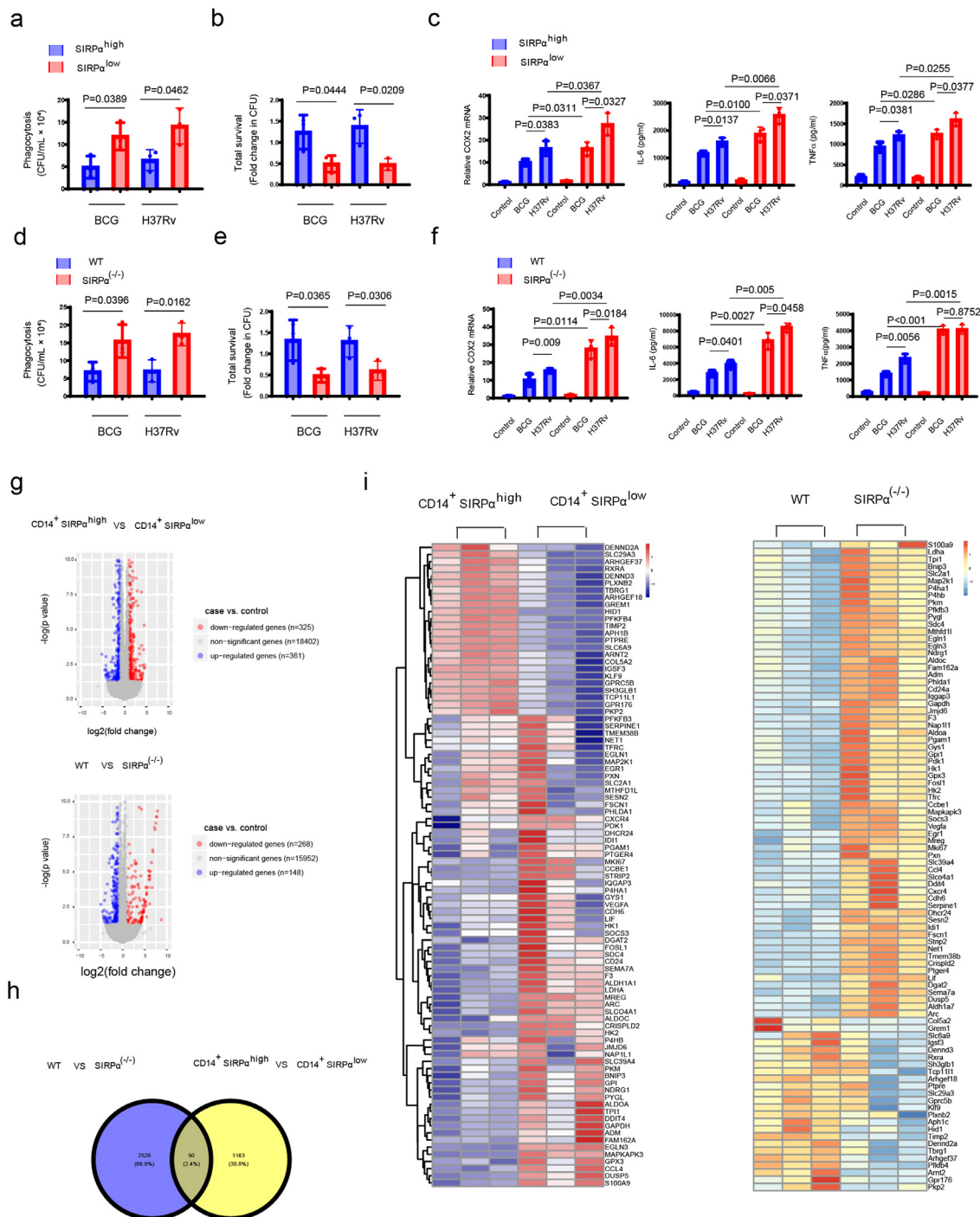


Figure 2. SIRP α suppresses the killing ability of macrophages against MTB. (a-b) CD14⁺ SIRP α ^{high} subset cells and CD14⁺ SIRP α ^{low} subset cells from three healthy controls were challenged with BCG or H37Rv at an MOI of 10. (a) phagocytosis and (b) killing activity of macrophages were quantified (student t-test). Each group was independently biological repeated for 3 times. (c) The cells prepared in (a-b) were harvested, and the mRNAs were analyzed for indicated targets by qRT-PCR, and the supernatants were analyzed for indicated targets by ELISA (student t-test). Each group was independently biological repeated for 3 times. (d-e) BMDMs from SIRP α ^{-/-} and wild type mice were incubated with GM-CSF (10 ng/ml) in vitro for 7 days, and then challenged with BCG or H37Rv at an MOI of 10. (d) phagocytosis and (e) killing activity of macrophages were quantified (student t-test). Each group was independently biological repeated for 3 times. (f) The cells prepared in (d-e) were harvested, and the mRNAs were analyzed for

against other intracellular bacteria, such as *Listeria* spp. (Supplementary Figure S4f-i, $P < 0.05$ for all, student t-test).

We then performed RNA-sequencing assays to determine transcriptional differences between $CD14^+SIRP\alpha^{high}$ and $CD14^+SIRP\alpha^{low}$ macrophages, and between wild type and $SIRP\alpha^{-/-}$ macrophages (Raw data was uploaded in <http://www.ncbi.nlm.nih.gov/bioproject/848343>, BioProject ID: PRJNA848343). Volcano plot displays the number of genes with significant differences between human $CD14^+SIRP\alpha^{high}$ macrophages and $CD14^+SIRP\alpha^{low}$ macrophages and between mice WT and $SIRP\alpha^{-/-}$ macrophages (Figure 2g). The identified targets varied greatly between humans and mice, and therefore we used a Venn graph to identify the overlapping series (Figure 2h). The clustering of the overlapping targets revealed that besides the cytokines, $SIRP\alpha$ might also regulate the expression of autophagy- and necrosis-related genes (Figure 2i).

$SIRP\alpha$ deficiency blocks necroptosis to enhance the killing against MTB

RNA-sequencing results suggested that $SIRP\alpha$ regulates macrophages necrosis. Consistently, propidium (PI) staining demonstrated that $SIRP\alpha^{-/-}$ macrophages showed less H37Rv induced necrosis than WT macrophages (Figure 3a, $P < 0.001$, student t-test). In MTB infection, macrophage necrosis is typically accompanied by extracellular bacterial spread.¹⁸ Here, extracellular MTB loads were slightly lower in $SIRP\alpha^{-/-}$ macrophages 4 days after infection, which is correlated with the necrosis rate (Figure 3b, $P = 0.0379$, student t-test).

Necroptosis is a type of programmed necrosis that requires signalling through a Receptor-interacting protein kinase 1 (RIPK1)/Receptor-interacting protein kinase 3 (RIPK3)/ Mixed lineage kinase domain-like (MLKL)-dependent pathway.¹⁹ CYLD is an important necroptosis element and has been reported to be cleaved by Lipopolysaccharides (LPS).¹⁹ Western blot here confirmed that H37Rv stimulation had similar effect on CYLD as LPS, and CYLD level was decreased in $SIRP\alpha^{-/-}$ macrophages under both LPS ($P < 0.001$, student t-test) and H37Rv ($P < 0.001$, student t-test) stimulation (Figure 3c-d). Meanwhile, we found that RIPK1^{-/-} and RIPK3^{-/-} macrophages decreased the total MTB survival rate at 24 h after the BCG, H37Rv, or clinical

MTB strains challenge when compared to the wild type controls (Supplementary Figure S5a-b, $P < 0.05$ for all, student t-test), indicating that necroptosis inhibition is a benefit for MTB killing, which is consistent with a previous report.¹⁸ These above results lead us to ask whether necroptosis pathway mediates the $SIRP\alpha$ function on MTB.

Cells undergo necroptosis when stimulated with low doses of LPS or bacteria in the presence of benzoyloxycarbonyl-Val-Ala-Asp-fluoromethyl ketone (zVAD-fmk).¹⁹ In this study, we found that the necroptosis marker, phosphorylated MLKL, was significantly induced by a low dose of LPS (1 ng/mL) or H37Rv (0.1 MOI) stimulation, and it was decreased in $SIRP\alpha^{-/-}$ macrophages, compared with the wild type group ($P < 0.001$ for both LPS and H37Rv treatment, student t-test), whereas the expression of total MLKL ($P = 0.5462$ for LPS treatment and $P = 0.7768$ for H37Rv treatment, no statistical difference) was not affected (Figure 3e-f). Similarly, LPS- or H37Rv-induced necroptosis was significantly attenuated in $SIRP\alpha^{-/-}$ macrophages, compared with the wild type controls (Figure 3g-h, $P < 0.001$ for both LPS and H37Rv treatment, student t-test). We blocked the necroptosis with a RIPK1 inhibitor, Necrostatin-1 (NEC-1), and the data indicated that blocking necroptosis could enhance the phagocytosis ($P = 0.3438$, no statistical difference) bactericidal ability ($P = 0.5322$, no statistical difference) of wide type (WT) and $SIRP\alpha^{-/-}$ macrophages to similar levels (Figure 3i-j). These results indicated that necroptosis plays an essential role in mediating the $SIRP\alpha$ functions on bactericidal ability.

$SIRP\alpha$ deficiency triggers autophagy of macrophages under MTB infection

On the other hand, autophagy has been reported as one of the most important means to combat exogenous infections.²⁰ Since the RNA-sequencing results from Figure 2g showed that autophagic process might also be regulated by $SIRP\alpha$, we therefore explored the role of autophagy in MTB infection. Figure 4a-b showed that $SIRP\alpha^{-/-}$ could enhance the co-localization of H37Rv with microtubule-associated protein 1 light chain 3 (LC3) positive autophagosomes ($P = 0.0250$) and lysosomal-associated membrane protein 1 (LAMP1) positive lysosomes ($P = 0.0193$), as revealed by confocal microscopy. Furthermore, the

indicated targets by qRT-PCR, and the supernatants were analyzed for the indicated targets by ELISA (student t-test). Each group was independently biological repeated for 3 times. (g) The cells prepared in (a-b and c-d) were challenged with H37Rv at an MOI of 10 for 24 h. The cells were harvested, and the total RNA samples were used to perform the RNA-seq experiment (Raw data was uploaded in <http://www.ncbi.nlm.nih.gov/bioproject/848343>, BioProject ID: PRJNA848343). Volcano plot displays the number of genes with significant differences between $CD14^+SIRP\alpha^{high}$ subset cells and $CD14^+SIRP\alpha^{low}$ subset cells and between WT BMDMs and $SIRP\alpha^{-/-}$ BMDMs. Each group was independently biological repeated for 3 times. (h) Venn diagram showing the distribution of the overlapped dis-regulated targets in (g). (i) Heatmap analysis displaying the overlapped targets in (g).

Results are shown as means \pm SD of three experiments.

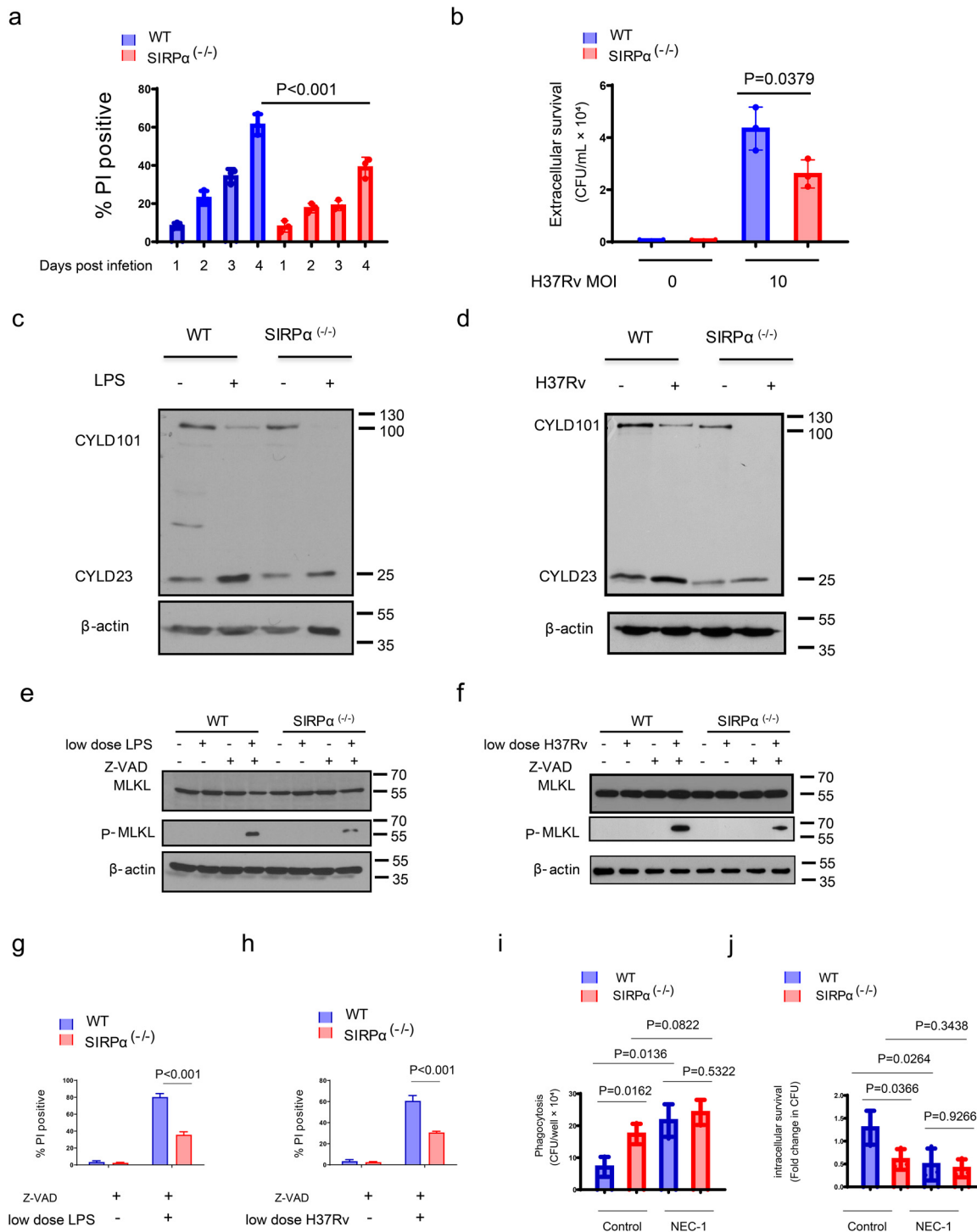


Figure 3. SIRPα deficiency blocks necroptosis to enhance the killing against MTB. (a) BMDMs from SIRPα^{-/-} and WT mice were incubated with GM-CSF (10 ng/ml) in vitro for 7 days, and then challenged with H37Rv for 0-4 days, and then the cells were used to determine the necrotic cell death rate by using propidium iodide (PI) stain (student t-test). Each group was independently biological repeated for 3 times. (b) The cells prepared in (a) were challenged with H37Rv for 4 days, and then the extracellular bacteria were quantified (student t-test). Each group was independently biological repeated for 3 times. (c-d) The cells prepared in (a) were challenged with (a) LPS at 200 ng/mL or (b) H37Rv at an MOI of 10 for 24 h, and CYLD expression was determined by western blot. Each group was independently biological repeated for 3 times. The statistical significance of the difference was determined by student t-

expression of SQSTM1 increased within 18 h after H37Rv challenge ($P < 0.001$, student t-test), while significantly decreased in $SIRP\alpha^{-/-}$ macrophages when compared to wild type cells ($P < 0.001$, student t-test), and iNOS was enhanced ($P < 0.001$, student t-test) at the same time points (Figure 4c). Interestingly, treatment with the anti-inflammatory factor IL-4 reduced the SQSTM1 and iNOS expression significantly in the two groups to the same levels (Figure 4c, $P = 0.8329$, no statistical difference), indicating that SQSTM1 enhancement by $SIRP\alpha$ deficiency might be an inflammation-dependent event. Furthermore, the autophagy flux inhibitor bafilomycin A1 (Baf A1) was used to detect the effect of $SIRP\alpha$ on the autophagy marker LC3-II.²⁰ Here, we showed that Baf A1 increased LC3-II expression in $SIRP\alpha^{-/-}$ macrophages ($P < 0.001$, student t-test), compared with the WT macrophages (Figure 4d), indicating that $SIRP\alpha$ deficiency enhanced autophagy.

The relationship between $SIRP\alpha$ and autophagy is predictable, because the pro-inflammatory environment produced by $SIRP\alpha$ deficiency contributes to the occurrence of autophagy.²¹ However, it was initially unexpected that $SIRP\alpha$ deficiency could suppress necroptosis since many of $SIRP\alpha$ deficiency-induced cytokines, such as TNF α , have been reported to mediate the enhancement of necroptosis.¹⁸ Previous literatures reported that autophagy process inhibits the occurrence of necroptosis, while necroptosis process can promote autophagy, indicating that there is a negative feedback crosstalk between autophagy and necroptosis.²² Here, when we use 3-methyladenine (3-MA) to block autophagy, the enhanced phagocytosis and killing ability against H37Rv of $SIRP\alpha^{(-/-)}$ macrophage was partly reversed, but still higher than in wild type cells (Figure 4e-f, $P = 0.0476$ for phagocytosis and $P = 0.0430$ for killing ability), and interestingly, the phagocytosis and bactericidal ability of wild type and $SIRP\alpha^{-/-}$ macrophages was enhanced to similar level ($P = 0.4041$ for phagocytosis and $P = 0.8700$ for killing ability, no statistical difference) after necroptosis was blocked by NEC-1, no matter whether 3-MA was added or not (Figure 4e-f), suggesting that necroptosis decreasing, rather than autophagy enhancement, is the main way to mediate $SIRP\alpha^{-/-}$ function against MTB.

$SIRP\alpha$ intracellular tail binds directly to PTK2B

The above experiments showed that $SIRP\alpha$ affects necroptosis and autophagy. Having clarified some of the

functional impacts of $SIRP\alpha$ deficiency in macrophages, we then sought to understand the direct molecular mechanisms behind its activity. $SIRP\alpha$ is a cell surface protein with an intracellular tail that contains the inhibitory ITIM motif domains.¹¹ To identify possible interaction partners of this domain, we used a CytoTrap yeast two-hybrid assay, in which the interaction between the target and the $SIRP\alpha$ intracellular tail occurs in the cytoplasm, in accordance with previous reports.²¹ Several positive clones were sequenced and identified by BLAST (Figure 5a). Protein tyrosine kinase 2B (PTK2B) (also called PYK2) was one of the positive targets and confirmed by the clone growth (Figure 5a-b), indicating that PTK2B has the potential to interact with $SIRP\alpha$ directly. We further confirmed the interaction by coimmunoprecipitation (Co-IP) of endogenously expressed $SIRP\alpha$ with PTK2B protein from mouse BMDMs, and this interaction could be enhanced under H37Rv treatment (Figure 5c, $P < 0.001$, student t-test). Next, we constructed the Flag-tagged full-length $SIRP\alpha$ vector, together with mutants carrying a deletion of 87 amino acids at the cytoplasmic tail ($SIRP\alpha\text{-}\Delta 87$) or specific phosphorylation site mutations in the ITIM domain (Figure 5d) and transfected them into 293T cells. Co-IP of exogenous $SIRP\alpha$ with endogenous PTK2B demonstrated that most of the phosphorylation site mutations in the ITIM domain could completely inhibit the binding of $SIRP\alpha$ and PTK2B ($P < 0.001$, student t-test). In contrast, the Y1 mutation could only slightly weaken the binding of these two proteins (Figure 5e, $P = 0.0479$, student t-test), indicating that the Y1 site has poor participation in $SIRP\alpha$ -PTK2B binding.

The inhibition of necroptosis and enhancement of killing against MTB by $SIRP\alpha$ deficiency requires PTK2B activities

We hypothesized that $SIRP\alpha$ might regulate PTK2B activities because of the binding. We found that PTK2B phosphorylation was significantly decreased under H37Rv treatment for 2 h ($P < 0.001$, student t-test), whereas the PTK2B phosphorylation levels were significantly higher in $SIRP\alpha^{-/-}$ macrophages ($P < 0.001$, student t-test), compared with the WT controls (Figure 6a). Meanwhile, the proteasome inhibitor MG132 (also a ubiquitination inhibitor) reversed the H37Rv function on PTK2B phosphorylation (Figure 6b, $P < 0.001$, student t-test). Furthermore, the ubiquitination degradation levels of PTK2B were decreased in the $SIRP\alpha^{-/-}$ group, compared with the wild type controls (Figure 6c,

test. (e-f) The cells prepared in (a) were challenged with a low dose of (e) LPS (1 ng/mL) or (f) H37Rv (MOI at 0.1), in combination with Z-VAD, and the cells were used to determine the total MLKL and MLKL phosphorylation levels by western-blotting. Each group was independently biological repeated for 3 times. The statistical significance of the difference was determined by student t-test. (g-h) The cells prepared in (e-f) were used to determine the necrotic cell death rate by using propidium iodide (PI) stain (student t-test). Each group was independently biological repeated for 3 times. (i-j) The cells prepared in (a) were challenged with H37Rv at an MOI of 10, without treatment, or with NEC-1. (i) phagocytosis and (j) killing activity of macrophages were quantified (student t-test). Each group was independently biological repeated for 3 times.

Results are shown as means \pm SD of three experiments.

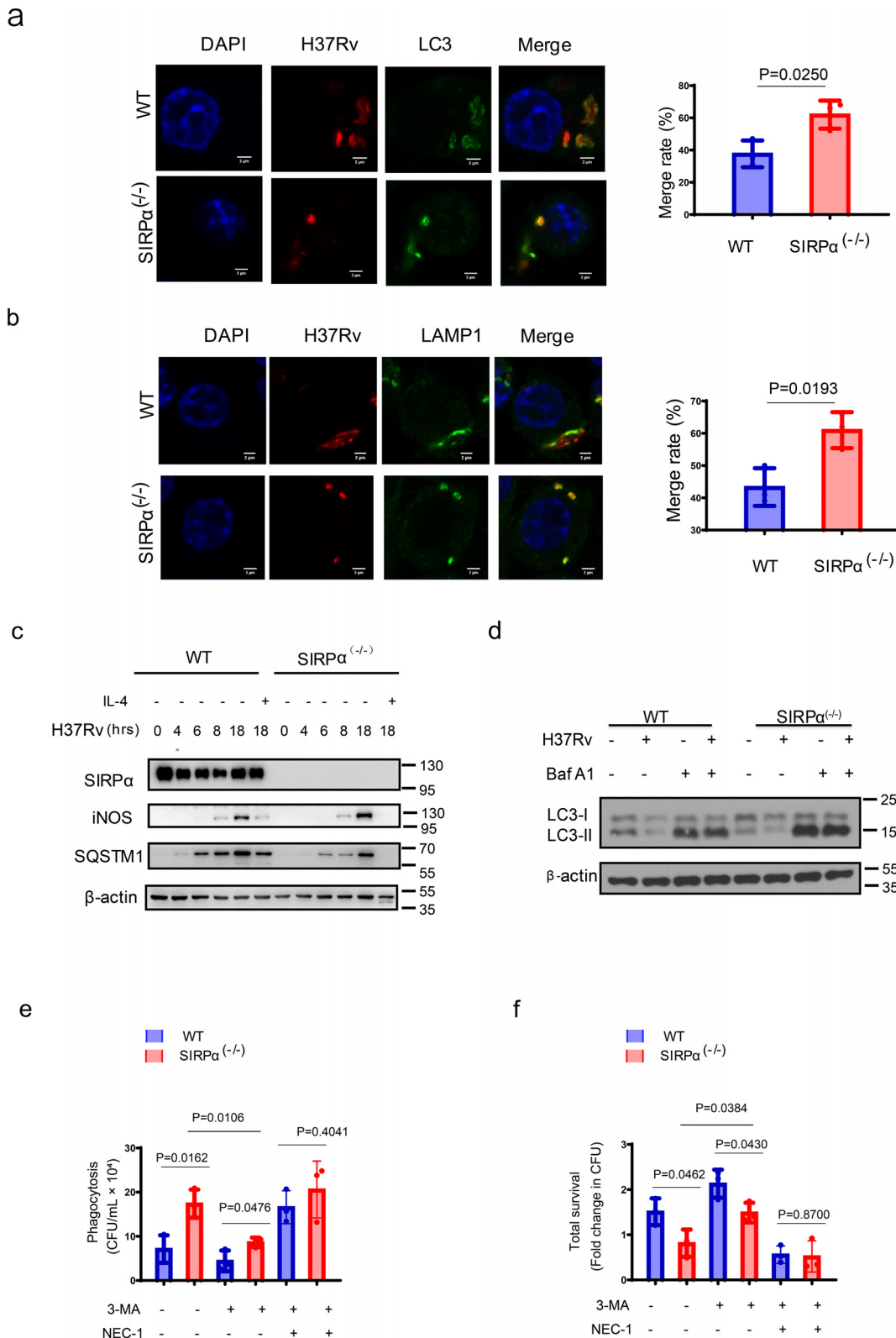


Figure 4. SIRP α deficiency promotes the formation of mycobacterial autophagosomes to enhance the killing ability of macrophages against MTB. (a-b) BMDMs from SIRP α ^(-/-) and WT mice were incubated with GM-CSF (10 ng/ml) in vitro for 7 days and

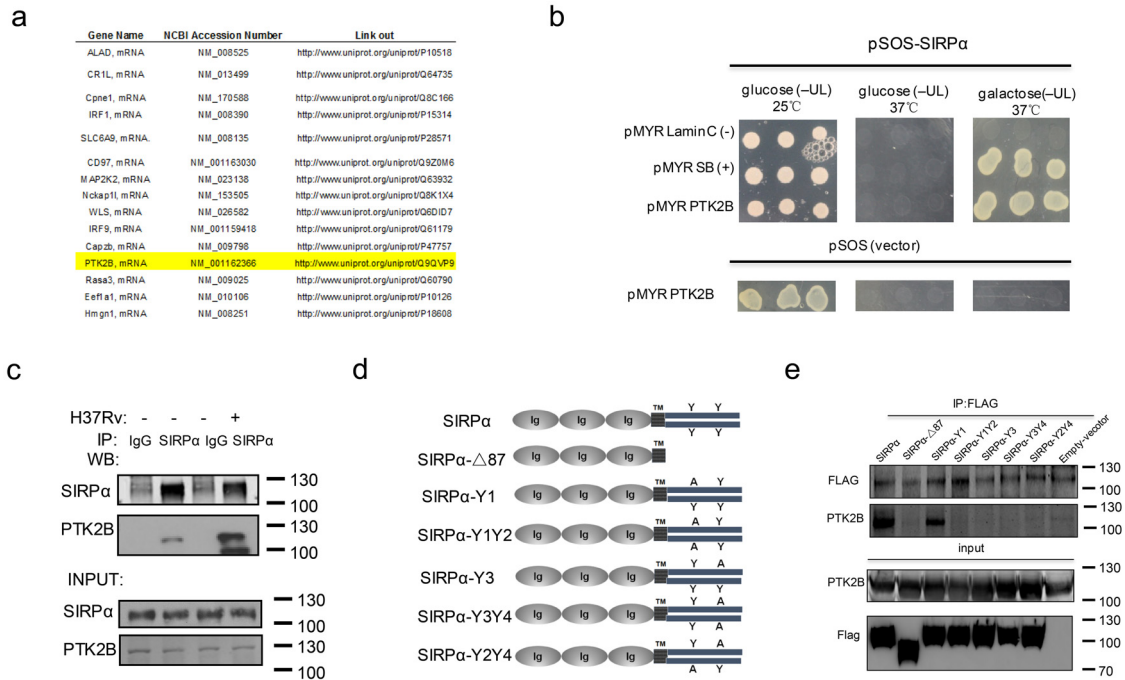


Figure 5. Identification of PTK2B as an interacting partner for SIRPα intracellular tail. (a) Mouse lung cDNA library in pMyr vector was co-transformed with pSOS-NUP98-HOXA9 (pSOS-SIRPα) into cdc25H yeast strain. Cytoplasmic yeast two-hybrid was performed, and the list of the positive cDNA clones was sequenced and identified by blast. Each group was independently biological repeated for 3 times. (b) Positive interaction between PTK2B and SIRPα was confirmed by cytoplasmic yeast two-hybrid. Plasmids of pMYR-PTK2B were isolated from yeast cells growing at 37°C in galactose containing medium and retransformed along with pSOS-NUP98-HOXA9 (pSOS-SIRPα) to confirm the interactions. Cells containing pSOS-NUP98-HOXA9 (pSOS-SIRPα) with pMYR-Lamin C or empty pSOS vector with pMyr-AESp (pMyr-PTK2B) were spotted as negative controls. Cells containing pSOS-NUP98-HOXA9 (pSOS-SIRPα) with pMYR-SB were spotted as a positive control. Growth at 37°C in galactose containing medium indicates a positive interaction. Each group was independently biological repeated for 3 times. (c) Co-IP of SIRPα with PTK2B from the lysates of WT BMDMs treated with H37Rv at an MOI of 10 for indicated time point. Each group was independently biological repeated for 3 times. The statistical significance of the difference was determined by student t-test. (d) Constructions of full-length Flag-SIRPα vector, intracellular tail deletion Flag-SIRPα vector, and specific phosphorylation site mutation Flag-SIRPα vectors. Each group was independently biological repeated for 3 times. The statistical significance of the difference was determined by student t-test. (e) Co-IP of SIRPα with PTK2B from the lysates of HEK293T cells transfected with full-length Flag-SIRPα vector, intracellular tail deletion Flag-SIRPα vector, and specific phosphorylation site mutation Flag-SIRPα vectors. Each group was independently biological repeated for 3 times. The statistical significance of the difference was determined by student t-test.

$P < 0.001$, student t-test). The above results indicated that SIRPα deficiency upregulate the PTK2B phosphorylation and inhibit its ubiquitination degradation, and therefore play its biological and immunological functions.

We randomly selected PTB patients with typical tuberculous pathological areas (caseous necrosis areas) in their lung tissues from the SIRPα-H group ($n = 16$) and in the SIRPα-L group ($n = 16$), respectively, and performed immunohistochemistry for SIRPα and P-

then stimulated with Texas Red-labelled H37Rv at an MOI of 10 for 1 h. Endogenous (A) LC3 or (B) LAMP1 was stained with antibodies followed by Alexa Fluor 488-conjugated IgG (Green). Left: representative merge of H37Rv with (a) autophagosomes (LC3 as marker) and (b) lysosomes (LAMP1 as marker) detected by confocal microscopy. Right: columnar statistics of merge rate (student t-test). Each group was independently biological repeated for 3 times. (c) The cells prepared in (a-b) were challenged with H37Rv at an MOI of 10, in combination with IL-4 or not at the indicated time point, and indicated target expressions were determined by western blotting. Each group was independently biological repeated for 3 times. The statistical significance of the difference was determined by student t-test. (d) The cells prepared in (a-b) were stimulated with H37Rv at an MOI of 10, in combination with or without Baf A1 for 24 h, and then LC3-I/II levels were detected by western blot. Each group was independently biological repeated for 3 times. The statistical significance of the difference was determined by student t-test. (e-f) The cells prepared in (a-b) were stimulated with H37Rv at an MOI of 10, in combination with 3-MA or NEC-1. (e) phagocytosis and (f) killing activity of macrophages were quantified (student t-test). Each group was independently biological repeated for 3 times.

Results are shown as means \pm SD of three experiments.

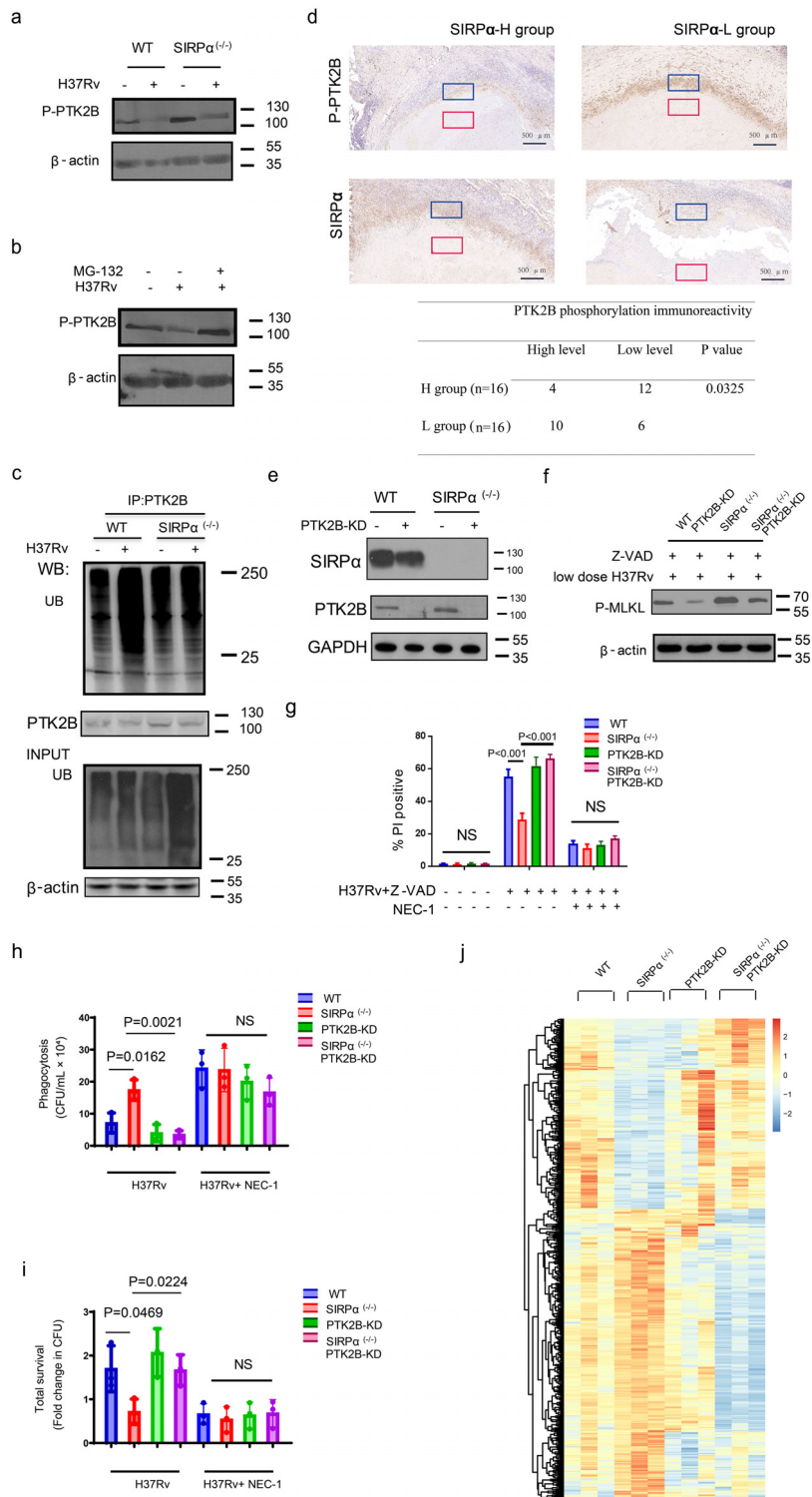


Figure 6. Inhibition of necroptosis and enhancement of killing ability against mycobacterial by SIRP α deficiency requires PTK2B activities. (a) BMDMs from SIRP α ^{-/-} and WT mice were incubated with GM-CSF (10 ng/ml) in vitro for 7 days and then challenged with H37Rv at an MOI of 10 for 2 h, and the PTK2B phosphorylation was detected by western blot. Each group was independently biological repeated for 3 times. The statistical significance of the difference was determined by student t-test. (b) BMDMs from WT mice were incubated with GM-CSF (10 ng/ml) in vitro for 7 days and then challenged with H37Rv at an MOI of 10, together

PTK2B. Generally, both is highly expressed at the edge of caseous necrotic structure, and low in the necrotic interior (Figure 6d, supplementary figure S6a-b). The phosphorylation levels of PTK2B were negatively correlated with the expression of SIRP α , based on the IRS score (Figure 6d, $P = 0.0325$, student t-test), which is consistent with the cytological results.

Since the results above indicated the importance of PTK2B in the function of SIRP α , we transfected PTK2B small interfering RNA (siRNA) (named PTK2B-KD) into WT and SIRP $\alpha^{-/-}$ macrophages. Western blotting assay confirmed the depletion of the PTK2B protein expression in the wild type and SIRP $\alpha^{-/-}$ macrophages (Figure 6e, $P < 0.001$, student t-test). Based on this cell model, we confirmed that the MLKL phosphorylation levels decreasing by SIRP α deficiency required PTK2B activity (Figure 6f, $P < 0.001$, student t-test). Meanwhile, necroptosis inhibition by SIRP α deficiency was reversed in SIRP $\alpha^{-/-}$ PTK2B-KD cases ($P < 0.001$, student t-test), whereas under NEC-1 treatment, the necroptosis rate of wild type, SIRP $\alpha^{-/-}$, PTK2B-KD, and SIRP $\alpha^{-/-}$ PTK2B-KD macrophages decreased and tended to be similar (Figure 6g, $P > 0.05$, not significant). Similar to the trend of the necroptosis rate, the phagocytosis and killing ability inhibition by SIRP α deficiency was reversed in SIRP $\alpha^{-/-}$ PTK2B-KD cases ($P = 0.0021$ for phagocytosis and $P = 0.0224$ for killing ability, student t-test), whereas under NEC-1 treatment, the bacterial load of the wild type, SIRP $\alpha^{-/-}$, PTK2B-KD, and SIRP $\alpha^{-/-}$ PTK2B-KD macrophages decreased and tended to be similar (Figure 6h, $P > 0.05$ for all, not significant), indicating that the function of SIRP α deficiency against intracellular MTB requires necroptosis inhibition by PTK2B activation. Besides, RNA-sequencing data demonstrated that of the genes

significantly regulated by SIRP α , a total of 488 targets (19.0%) could be reversed in SIRP $\alpha^{-/-}$ PTK2B-KD cases, indicating that many SIRP α -related signalling, including phagocytosis and intracellular tuberculosis killing pathways, are mediated by PTK2B (Figure 6i, $P < 0.05$ for all, student t-test).

Even if the above results indicated the involvement of the SIRP α /PTK2B axis in PTB, the involvement of the SIRP α /PTK2B axis in necroptosis remained to be elucidated. Therefore, we tested several key proteins involved in necroptosis for the ability to bind to PTK2B in order to elucidate the possible regulatory role of the SIRP α /PTK2B axis on necroptosis. Co-IP assays demonstrated that PTK2B could bind to RIPK1 on its death domain directly (Figure 7a, $P < 0.001$, student t-test), and this association was confirmed by co-localization of the RIPK1 death domain with PTK2B, as determined by a confocal microscopy assay (Figure 7b, $P < 0.001$, student t-test). Previous reports demonstrated that proteins binding to the RIPK1 death domain could inhibit the RIPK1 activation and therefore block RIPK1-mediated necroptosis.²³ Here, we found that in PTK2B-KD macrophages, the RIPK1 phosphorylation levels were significantly higher than that in wild type controls (Figure 7c, $P < 0.001$, student t-test). Necroptosis was also proved to be induced by PTK2B-KD transfection ($P = 0.0011$, student t-test) through a RIPK1-dependent manner (Figure 7d). Collectively, the above results suggest that SIRP α -PTK2B binding might impact the PTK2B activities. SIRP α knockout thus activated PTK2B activation and decreased the necroptosis processing in macrophage by relieving the inhibitory effect of PTK2B on RIPK1 (Figure 8).

with or without MG-132 for 2 h, and the PTK2B phosphorylation was detected by western blot assay. Each group was independently biological repeated for 3 times. The statistical significance of the difference was determined by student t-test. (c) The cells prepared in (a) were challenged with H37Rv at an MOI of 10 for 2 h, and Co-IP was performed on the two groups of cells by the anti-PTK2B antibody. PTK2B and ubiquitin were detected by western blot. Each group was independently biological repeated for 3 times. The statistical significance of the difference was determined by student t-test. (d) PTB patients with typical tuberculous pathological areas (caseous necrosis areas) in their lung tissues from the SIRP α -H group ($n=16$) and in the SIRP α -L group ($n=16$) were randomly selected, respectively, and PTK2B phosphorylation and SIRP α expression staining were determined by immunohistochemistry. (Upper panel) Representative immunohistochemical field of vision. Scale bars, 500 μ m; (Lower panel) Negative correlation between PTK2B phosphorylation and SIRP α expression in these patients (Pearson's Chi-square test). (e) Western blot confirmed the SIRP α and PTK2B levels in SIRP $\alpha^{-/-}$ PTK2B-KD, PTK2B-KD, SIRP $\alpha^{-/-}$ and wild type macrophages. Each group was independently biological repeated for 3 times. The statistical significance of the difference was determined by student t-test. (f-g) SIRP $\alpha^{-/-}$ PTK2B-KD, PTK2B-KD, SIRP $\alpha^{-/-}$, and wild type macrophages were challenged with H37Rv at an MOI of 0.1, in combination with Z-VAD for 24h, and then (f) the p-MLKL levels were determined by western blotting assay (The statistical significance of the difference was determined by student t-test.); (g) the necrotic cell death rate was determined by propidium iodide (PI) staining (student t-test). Each group was independently biological repeated for 3 times. (h-i) SIRP $\alpha^{-/-}$ PTK2B-KD, PTK2B-KD, SIRP $\alpha^{-/-}$, and wild type macrophages were challenged with H37Rv at an MOI of 10, in combination with NEC-1. (h) phagocytosis and (i) killing activity of macrophages were quantified (student t-test). Each group was independently biological repeated for 3 times. (j) The cells prepared in (h-i) were challenged with H37Rv at MOI of 10 for 24 h, and the cells were harvested, and their RNA samples were used to perform the RNA-seq experiment (Raw data was uploaded in <http://www.ncbi.nlm.nih.gov/bioproject/848343>, BioProject ID: PRJNA848343). Each group was independently biological repeated for 3 times.

Results are shown as means \pm SD of three experiments.

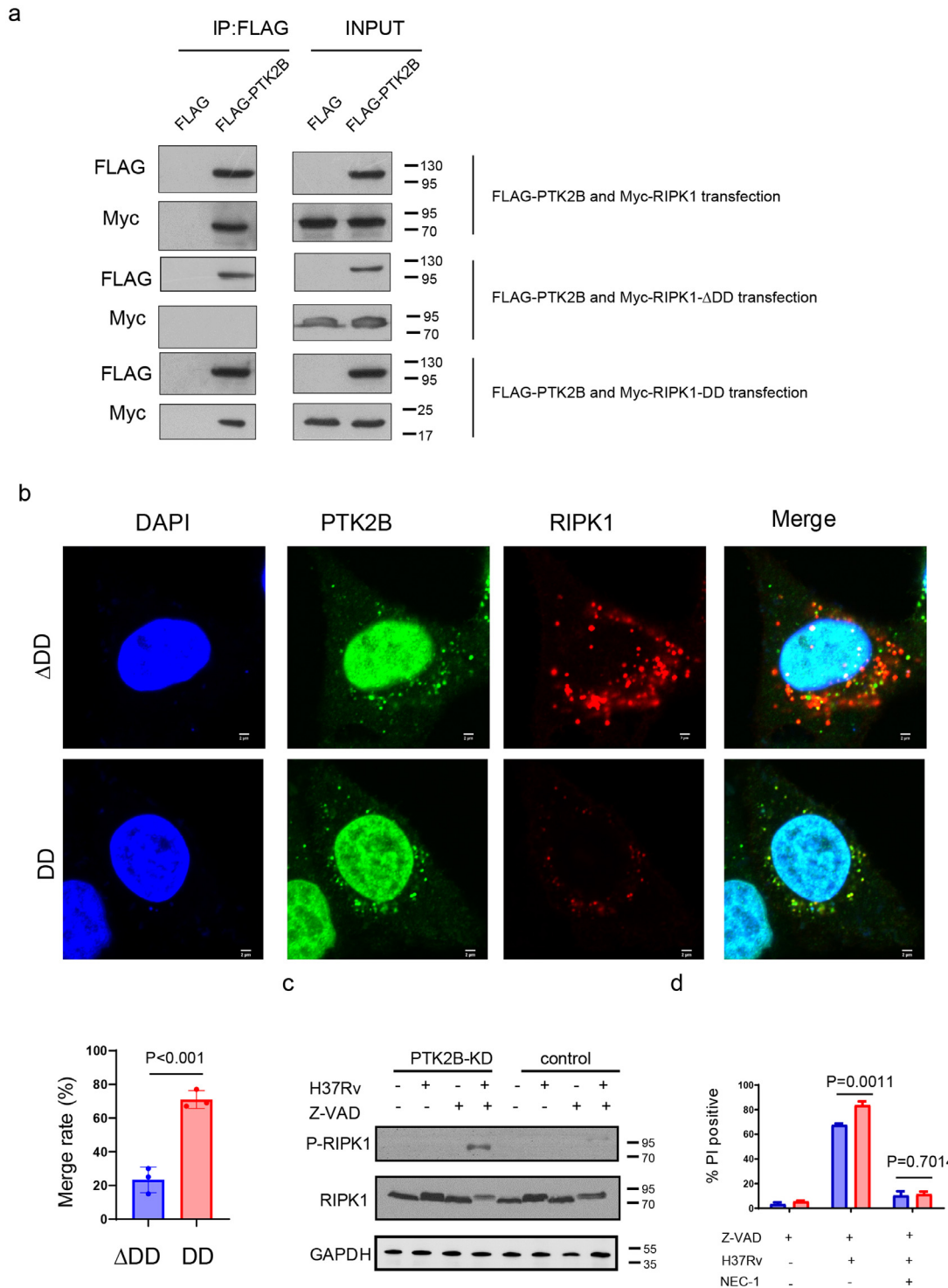


Figure 7. PTK2B binds to the death domain of RIPK1 to inhibit the necroptosis process. (a) Co-IP of exogenous PTK2B with RIPK1 from the lysates of HEK293T cells transfected with Myc-RIPK1 (full length), Myc-RIPK1-DD (death domain), and Myc-RIPK1- Δ DD (death domain deletion), in combination with Flag-PTK2B. Each group was independently biological repeated for 3 times. The statistical significance of the difference was determined by student t-test. (b) HEK293T cells were transfected with Myc-RIPK1-DD and Myc-RIPK1- Δ DD, in combination with Flag-PTK2B. Exogenous PTK2B was stained with Flag antibodies followed by Alexa Fluor 488-conjugated IgG (Green), and RIPK1 were stained with Myc antibodies followed by AF-647-conjugated IgG (Red). (Upper panel)

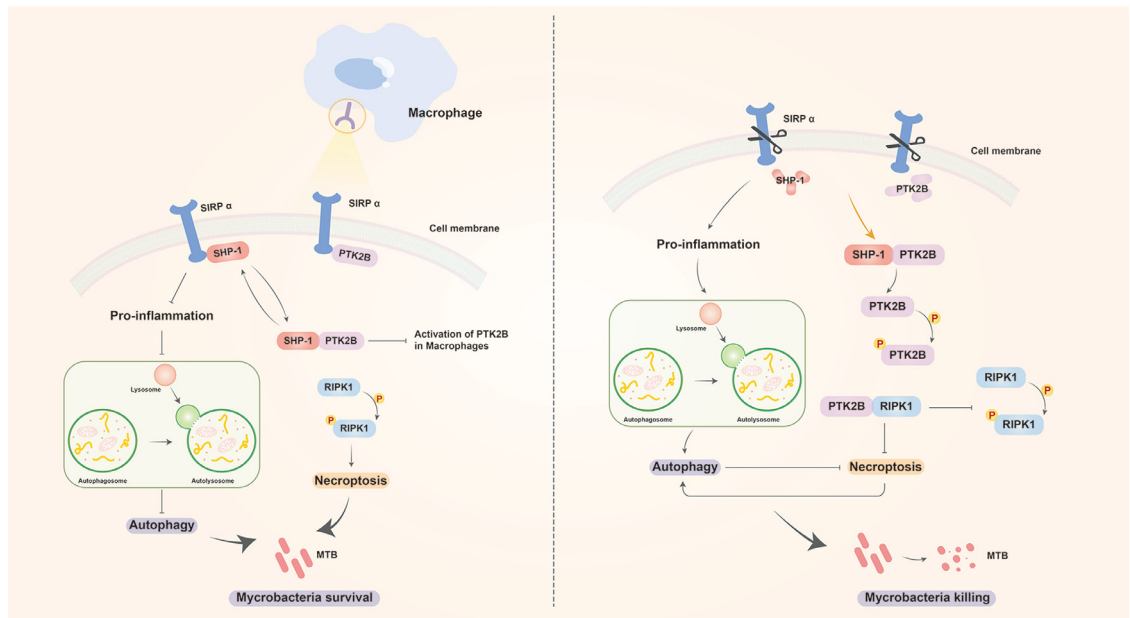


Figure 8. The mechanistic schematic model of the role of SIRP α in macrophage-MTB interaction. Briefly, SIRP α -PTK2B binding impact the PTK2B activities. SIRP α knockout thus activated PTK2B activation and decreased the necroptosis processing in macrophage by relieving the inhibitory effect of PTK2B on RIPK1.

Adoptive transfer of SIRP α -deficient macrophage transplants enhances the killing ability against MTB pathogenesis in mouse models

To assess the killing effects of SIRP α against the MTB in vivo, we generated SIRP $\alpha^{-/-}$, PTK2B-KD, and SIRP $\alpha^{-/-}$ PTK2B-KD macrophages mouse models using bone marrow transplantation, which has been shown to mediate donor engraftment of macrophages by more than 90%, according to a previous report.²⁴ Wild type mice were reconstituted with wild type (WT \rightarrow WT), SIRP $\alpha^{-/-}$ (SIRP $\alpha^{-/-}$ \rightarrow WT), PTK2B-KD (PTK2B-KD \rightarrow WT), or SIRP $\alpha^{-/-}$ PTK2B-KD (SIRP $\alpha^{-/-}$ PTK2B-KD \rightarrow WT) macrophages and then were infected with BCG or H37Rv. A decrease in bacterial load in the lungs was seen in SIRP $\alpha^{-/-}$ \rightarrow WT mice at 28 days after BCG or H37Rv infection ($P=0.0017$ for BCG and $P<0.001$ for H37Rv, student t-test), whereas SIRP $\alpha^{-/-}$ PTK2B $^{-/-}$ \rightarrow WT could reverse ($P=0.0011$ for BCG and $P<0.001$ for H37Rv, student t-test) this effect (Figure 9a-b). The results indicate that SIRP α deficient macrophage transplant enhances the killing ability against MTB in vivo. Nevertheless, we also found

that the side effect of this treatment is that it may increase the inflammatory damage caused by MTB infection. The analysis of total lung mRNA expression at 3 days after BCG infection revealed that SIRP $\alpha^{-/-}$ \rightarrow WT produced more TNF α and IL-6 and that SIRP $\alpha^{-/-}$ PTK2B $^{-/-}$ \rightarrow WT could reverse this regulation (Figure 9c-d, $P<0.05$ for all, student t-test). One side effect is that SIRP $\alpha^{-/-}$ \rightarrow WT resulted in a larger inflammatory area of infected lungs in a PTK2B-dependent manner (Figure 9e-g, $P<0.001$, student t-test).

Urinary trypsin inhibitor (ulínastatin) is widely used to block inflammatory damage. In this study, ulínastatin was used to pretreat SIRP $\alpha^{-/-}$ \rightarrow WT mice, followed by BCG or H37Rv infection. Ulinastatin had no effect on the control effect of SIRP $\alpha^{-/-}$ \rightarrow WT on mycobacteria load (Supplementary Figure 7a-b, $P = 0.8146$ for BCG and $P = 0.8757$ for H37Rv) but could significantly down-regulate the TNF α and IL-6 mRNA levels (Supplementary Figure 7c-d, $P<0.001$ for all, student t-test) and decrease the inflammatory area (Supplementary Figure 7e, $P<0.001$ for all, student t-test) in the lungs of the

representative merge of PTK2B with RIPK1 detected by confocal microscopy. (Lower panel) columnar statistics of merge rate (student t-test). Each group was independently biological repeated for 3 times. (c) PTK2B-KD and WT macrophages were challenged with H37Rv at an MOI of 0.1, in combination with Z-VAD for 24 h, and then the total RIPK1 and RIPK1 phosphorylation levels were determined by western blotting assay. Each group was independently biological repeated for 3 times. The statistical significance of the difference was determined by student t-test. (d) PTK2B-KD and WT macrophages were challenged with H37Rv at an MOI of 0.1, in combination with Z-VAD for 24 h, in combination with NEC-1. The necrotic cell death rate was determined by propidium iodide (PI) staining (student t-test). Each group was independently biological repeated for 3 times.

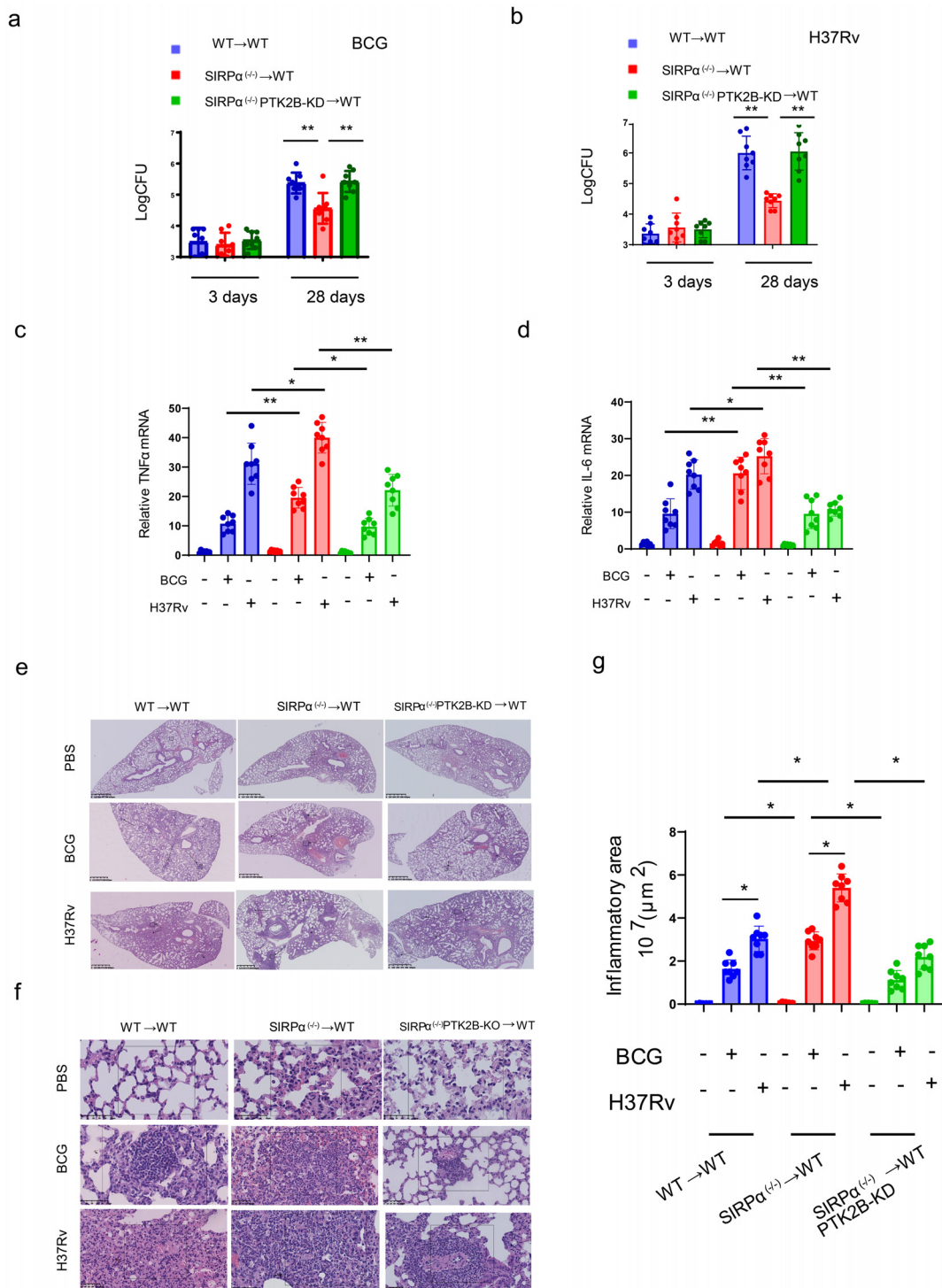


Figure 9. SIRP α deficiency BMDM transplantation enhances the killing ability against BCG in mice. (a-b) WT→WT, SIRP α ^{-/-}→WT, PTK2B^{-/-}→WT, or SIRP α ^(+/−)PTK2B^{-/-}→WT mice were infected by (a) BCG, or (b) H37Rv, and the tuberculosis CFU counting in lung tissue was determined (student t-test). Each treatment group was composed of eight mice. (c-d) Cytokines in the lungs from the mice described in (A-B) were determined by qRT-PCR 3 days after infection (student t-test). (e-g) The histopathology of the lungs from the mice described in (A-B) was determined by HE stain 28 days after infection. Scale bars (E) 625 μm; (F) 50 μm. (G) Inflammatory areas were calculated from the tissues (student t-test).

infected mice. The above results indicated that the combination of ulinastatin and $\text{SIRP}\alpha^{-/-} \rightarrow \text{WT}$ might be a potential anti-MTB regimen.

Discussion

Blood-based biomarkers for PTB have many benefits, such as relative ease of collection, short detection period, simple laboratory requirements, and safety of detectors. The initial goal of this work was to identify novel blood diagnostic and prognostic biomarkers for PTB. Many previous efforts have been forwarded to develop PTB biomarkers through genome-wide detection (RNA-sequencing and microarray) (Supplementary Table 1). Such studies acknowledged a variety of limitations, including being single-center studies and using a single platform, which lacks reproducibility and robustness.²⁵ By using a meta-analysis, we implemented a cross-platform integration, which yielded a series of dysregulated targets in patients with PTB. As expected, MTB infection promotes the secretion of a large number of pro-inflammatory factors. The KEGG analysis and a review of the literature revealed that $\text{SIRP}\alpha$, one of the negative regulators of immunity, was also significantly upregulated. This result gave us an important hint: the immune escape ability of MTB might be partly achieved by the upregulation of $\text{SIRP}\alpha$ in macrophages. If so, $\text{SIRP}\alpha$ expression patterns might be specific to PTB patients, thus differentiating PTB from other diseases such as cancers because previous reports demonstrated that $\text{SIRP}\alpha$ was significantly decreased in several cancer types, compared with healthy controls.^{26,27} qRT-PCR results of all the genes summarized in Figure 1B against a small number of clinical samples showed that $\text{SIRP}\alpha$ was the only target with the opposite expression trend in PTB and NSCLC, which preliminarily confirmed our prediction. Through analysis of data from multiple centers, we observed that $\text{SIRP}\alpha$ -positive macrophages and $\text{SIRP}\alpha$ expression were at higher levels in PBMCs and BAL from PTB patients when compared with that of HCs or NSCLC patients. PTB and NSCLC are very similar in the early stage of onset and are challenging to differentiate. This work suggests that it is possible to differentiate the two diseases based on $\text{SIRP}\alpha$ expression. Moreover, $\text{SIRP}\alpha$ expression could also distinguish PTB patients from pneumonia and latent infection.

Previous literatures reported that bacteria and LPS can regulate $\text{SIRP}\alpha$ expression by regulating TLR/NF-kappaB signalling pathway.²³ As we know, MTB also interacts with macrophage by recognizing and acting on the TLR. Therefore, TLR/NF-kappaB may be an important way to mediate the regulation of $\text{SIRP}\alpha$ expression by MTB. It was pointed out that there are multiple signalling pathways regulating $\text{SIRP}\alpha$ expression.²³ Our ongoing work also found some immunomodulator can

regulate $\text{SIRP}\alpha$ expression (data not shown). Therefore, how MTB regulates $\text{SIRP}\alpha$ needs further study.

As seen in previous studies,^{12,24} our findings demonstrated that $\text{SIRP}\alpha$ deletion enhances the production of inflammatory factors and the clearance of pathogens in macrophage and in mouse models. Since $\text{SIRP}\alpha$ negatively regulates various biological functions, these results were expected. Nevertheless, this result was not enough to fully elucidate the regulatory role of $\text{SIRP}\alpha$ in host organisms. As we know, macrophages can be generally differentiated into classically activated macrophages (M1) or alternatively activated macrophages (M2) in response to microbial stimuli,²⁸ but there are many more different macrophage subsets according to the expression characteristics of surface markers.²⁹ Even in the same person's blood, there are multiple macrophage subtypes at the same time. The highlight of our work is that we elucidated that the $\text{CD14}^+\text{SIRP}\alpha^{\text{low}}$ macrophage subsets play the primary killing role against pathogenic bacteria in human blood. This explains why $\text{SIRP}\alpha^{\text{high}}$ macrophages correlated with poor treatment outcomes of patients with PTB. RNA sequencing determination with both human ($\text{CD14}^+\text{SIRP}\alpha^{\text{high}}$ vs. $\text{CD14}^+\text{SIRP}\alpha^{\text{low}}$) and mice macrophages (WT vs. $\text{SIRP}\alpha^{-/-}$), followed by functional clustering of differential genes, identified new cellular functions regulated by $\text{SIRP}\alpha$. Notably, autophagy and necroptosis were confirmed to be $\text{SIRP}\alpha$ -regulated cell processes that are required in intracellular MTB clearance.

Autophagy has been demonstrated as a novel mechanism to kill bacteria, and numerous studies emphasize a role for autophagy in macrophages during MTB infection.^{17,20,30,31} Necrotic cell death, which can be triggered by $\text{TNF}\alpha$ under certain conditions, has been reported to result in tissue damage and granuloma formation.^{32,33} Generally, both autophagy and necrosis are enhanced by excess inflammation, and they, in turn, could affect each other.³⁴ Nevertheless, in the present study, we confirmed that $\text{SIRP}\alpha$ deletion promoted the autophagy process but inhibited programmed necrosis. It will be interesting to explore how necroptosis was blocked when many of the necroptosis factors, such as $\text{TNF}\alpha$ and iNOS, were enhanced in $\text{SIRP}\alpha$ -knockout macrophages.

The intracellular region of $\text{SIRP}\alpha$ contains two ITIMs with four tyrosine residues phosphorylated in response to stimuli. This region plays an important role in transmitting downstream signals.⁸ The CytoTrap yeast two-hybrid assay and co-IP demonstrated that PTK2B was a promising target, which could bind to the intracellular region of $\text{SIRP}\alpha$. Our results indicate that $\text{SIRP}\alpha$ deletion increased the association of SHP1 with PTK2B, leading to the activation of PTK2B. Geng et al.³⁵ reported that in a hepatocellular carcinoma cell line, overexpression of PTK2B resulted in transfectants developing less necrosis and apoptosis. In this study,

we found that PTK2B knockout enhanced necroptosis in wild type macrophages. Meanwhile, the suppression of necroptosis by SIRP α knockout requires PTK2B, suggesting that PTK2B activation might be the cause of SIRP α -knockout-induced necroptosis. PTK2B has been reported to interact with SHP-1 and Src, and this might play an important role in various macrophage functions.³⁶ While normal SIRP α expression might act to sequester SHP-1 and PTK2B separately, the ablation of SIRP α expression might release both proteins to freely interact to influence necroptosis. After all, several reports have demonstrated that the Src family is involved in necroptosis,^{37,38} and other PTK2B interaction partners such as Calmodulin-dependent kinase II (CaMKII) are also associated with necroptosis.³⁹ Nevertheless, we did not find any direct evidence that PTK2B mediates the regulation of necroptosis. In this study, we found that PTK2B could directly target the RIPK1-DD. Meng et al.²³ showed that RIPK1-DD mediated the activation of RIPK1 to control necroptosis and other cell death types. Kurenova et al.⁴⁰ confirmed that proteins binding to RIPK1-DD could negatively regulate the RIPK1 activation and suppress RIPK1-mediated cell death. Our results, combined with these previous reports, indicated that SIRP α -PTK2B-RIPK1 is a new and promising necroptosis-related cell death signaling. This result can explain the molecular mechanism of SIRP α regulating PTB progression since we confirmed the important role of necroptosis in the bactericidal effect of macrophages against MTB. On the other hand, this finding can also be used for reference in the study of tumour cell survival and death switch regulation.

Different cell death forms have different effects on host-MTB interaction. Generally, apoptosis and autophagy positively mediate the sterilization of macrophages against intracellular MTB, whereas necrosis is considered host detrimental. Behar et al have summarized the function of different type of cell death against tuberculosis, and indicated that necrosis could allow the pathogen to escape intracellular defence mechanisms and allows the pathogen to disseminate.⁴¹ Also, necroptosis is one of the principal pathological features of tuberculous granulomas, and a report by Roca et al.¹⁸ indicated that pharmacological interventions on the necroptosis pathway could act as host-targeting antituberculosis drugs. However in contrast, some reports indicated that necrosis might also be a crucial host defence to microbial infection, as well as being critical for organ development and cellular homeostasis in multicellular organisms.⁴² Meanwhile, some research groups showed that necroptosis could not affect the survival of tuberculosis in the host.⁴³ The opposite results may be because the authors used different models and different necroptosis stimuli. It also suggested that the mechanism of necroptosis in macrophages is complex and needs more extensive study.

Our cytological experiments indicated the positive antibacterial effect of SIRP α knockout genotype, but there are also contrary reports. Li et al.⁴³ found that SIRP α ^{-/-} could increase erythropoiesis as well as heightened susceptibility to Salmonella infection. reduce the amount of red blood cells and increased susceptibility to Salmonella infection, indicating that SIRP α might play different roles in different cell types. Therefore, we used macrophage transplantation technology to construct the mice model with SIRP α ^{-/-} macrophages (SIRP expression still exists in other cells). This study found that SIRP α ^{-/-} macrophages transplantation can play a stronger anti-TB activity than WT macrophages transplantation, which is consistent with the mechanistic findings of this study. One side effect of this method is that it will also cause more serious inflammatory damage, which might be induced by high level of pro-inflammatory cytokines secretions. Interestingly, we found that co-treatment with SIRP α ^{-/-} macrophages and ulinastatin, a commercial anti-inflammatory drug, could exert the curative effect of anti tuberculosis and anti-inflammatory at the same time, and this might provide a new way for PTB treatment.

In conclusion, the inhibitory effect of SIRP α on bactericidal activity leads to considering the possibility that the changes in SIRP α expression might be a prognosis indicator in MTB infection. We first found a negative correlation between SIRP α expression and phosphorylation of PTK2B in lung tissues of PTK2B patients. Interestingly, SIRP α expression was also associated with poor prognosis. Altogether, our results define SIRP α as a biomarker for MTB infection and underlying mechanisms for maintaining macrophage homeostasis through autophagy and necroptosis. SIRP α knockout plays a major role in killing MTB by weakening necroptosis. In addition, SIRP α knockout can improve the MTB killing activity of macrophages by strengthening autophagy, but only as an auxiliary or partial role, and SIRP α knockout weakens necroptosis and strengthens autophagy but through different pathway. Autophagy strengthening will also lead to necroptosis strengthening, which might cause by negative feedback. Those findings provide exciting insights into the pathogenesis of tuberculosis and suggest that novel therapeutics that block SIRP α might be beneficial in the management of MTB infection, opening a wealth of new possibilities in the treatment of PTB.

There are some limitations for this work, and the most important one is the sample size. We calculated sample size requirement by using subial module of PASS software, and obtained that the sample size required for this work was 146 cases. We first screened a series of candidate markers and found that SIRP α had the most advantage. This conclusion is based on a small number of samples testing. Similarly, we found that the expression of SIRP α can distinguish PTB from

pneumonia and lung cancer, which is also based on a small number of samples. In order to be more rigorous, these conclusions need to be verified based on large sample size testing in the subsequent study. We tested the correlation between SIRP α and clinical and prognostic indicators in PTB patients. The included sample size for the correlation determination of SIRP α and clinical and prognostic indicators of PTB patients is larger than the required sample size, and these samples are from 5 hospitals in 4 regions. However, it is still insufficient to fully reflect the relationship between SIRP α and clinical phenotypes of PTB patients in different regions in China. More regional participation and larger scale research are still needed. In addition, the dynamic changes of SIRP expression in tuberculosis patients also need further monitoring.

Contributors

HX, LD, DW and JH conceived and coordinated the study; DW, YL, FX, HZ, XZ, YH, GD and DL designed, performed and analyzed the experiments, wrote the paper. ZL, BS, YY, GM and ZT carried out the clinical data collection. AT and YL made and raised mice. DW performed the mice-based experiments and was aware of the group allocation at the different stages of the experiment. HX, LD, DW and JH have verified the underlying data. All authors read and approved the final version of the manuscript.

Data sharing statement

The datasets used and/or analysed during the current study are available from the corresponding author on reasonable request.

Declaration of interests

The authors declare that they have no conflict of interest.

Acknowledgements

We thank professor Ying Li (IRCBC, SIOC, Chinese Academy of Sciences,) for her providing us the pcDNA3.1-Myc-RIPK1, pcDNA3.1-Myc-RIPK1-DD, and pcDNA3.1-Myc-RIPK1-DD plasmids as gifts. This work was financially supported by the Chinese National Natural Science Foundation project (No.81401635).

Supplementary materials

Supplementary material associated with this article can be found in the online version at doi:10.1016/j.ebiom.2022.104278.

References

- Schluger NW. AJRCCM: 100-year anniversary. Focus on tuberculosis. *Am J Respir Crit Care Med.* 2017;195:1112–1114.
- Phillips PP, Davies GR, Mitchison DA. Biomarkers for tuberculosis disease activity, cure, and relapse. *Lancet Infect Dis.* 2010;10:69–70. author reply 70–61.
- Cao T, Lyu L, Jia H, et al. A two-way proteome microarray strategy to identify novel mycobacterium tuberculosis-human interactors. *Front Cell Infect Microbiol.* 2019;9:65.
- Barclay AN. Signal regulatory protein alpha (SIRPalph)/CD47 interaction and function. *Curr Opin Immunol.* 2009;21:47–52.
- Queval CJ, Brosch R, Simeone R. The macrophage: a disputed fortress in the battle against mycobacterium tuberculosis. *Front Microbiol.* 2017;8:2284.
- Tan S, Russell DG. Trans-species communication in the Mycobacterium tuberculosis-infected macrophage. *Immunol Rev.* 2015;264:233–248.
- Wallis RS, Kim P, Cole S, et al. Tuberculosis biomarkers discovery: developments, needs, and challenges. *Lancet Infect Dis.* 2013;13:362–372.
- Barclay AN, Van den Berg TK. The interaction between signal regulatory protein alpha (SIRPalph) and CD47: structure, function, and therapeutic target. *Annu Rev Immunol.* 2014;32:25–50.
- Waters WR, Palmer MV, Nonnecke BJ, et al. Signal regulatory protein alpha (SIRPalph) cells in the adaptive response to ESAT-6/CFP-10 protein of tuberculous mycobacteria. *PLoS One.* 2009;4:e6414.
- Bian Z, Shi L, Guo YL, et al. Cd47-Sirpalph interaction and IL-10 constrain inflammation-induced macrophage phagocytosis of healthy self-cells. *Proc Natl Acad Sci U S A.* 2016;113:E5434–E5443.
- van Beek EM, Zarate JA, van Bruggen R, et al. SIRPalph controls the activity of the phagocyte NADPH oxidase by restricting the expression of gp91(phox). *Cell Rep.* 2012;2:748–755.
- Baral P, Utaisincharoen P. Involvement of signal regulatory protein alpha, a negative regulator of Toll-like receptor signaling, in impairing the MyD88-independent pathway and intracellular killing of Burkholderia pseudomallei-infected mouse macrophages. *Infect Immun.* 2012;80:4223–4231.
- Li LX, Atif SM, Schmiel SE, Lee SJ, McSorley SJ. Increased susceptibility to Salmonella infection in signal regulatory protein alpha-deficient mice. *J Immunol.* 2012;189:2537–2544.
- Benjamini Y, Hochberg Y. Controlling the false discovery rate: a practical and powerful approach to multiple testing. *J R Stat Soc Ser B.* 1995;57:289–300.
- Paroha R, Chourasia R, Rai R, et al. Host phospholipase C- γ 1 impairs phagocytosis and killing of mycobacteria by J774A.1 murine macrophages. *Microbiol Immunol.* 2020;64:694–702.
- Amaral EP, Costa DL, Namasivayam S, et al. A major role for ferroptosis in Mycobacterium tuberculosis-induced cell death and tissue necrosis. *J Exp Med.* 2019;216:556–570.
- Kimmey JM, Huynh JP, Weiss LA, et al. Unique role for ATG5 in neutrophil-mediated immunopathology during M. tuberculosis infection. *Nature.* 2015;528:565–569.
- Roca FJ, Ramakrishnan L. TNF dually mediates resistance and susceptibility to mycobacteria via mitochondrial reactive oxygen species. *Cell.* 2013;153:521–534.
- Legarda D, Justus SJ, Ang RL, et al. CYLD proteolysis protects macrophages from TNF-mediated auto-necroptosis induced by LPS and licensed by type I IFN. *Cell Rep.* 2016;15:2449–2461.
- Gupta M, Shin DM, Ramakrishna L, et al. IRF8 directs stress-induced autophagy in macrophages and promotes clearance of Listeria monocytogenes. *Nat Commun.* 2015;6:6379.
- Sarma NJ, Yaseen NR. Amino-terminal enhancer of split (AES) interacts with the oncoprotein NUP98-HOXA9 and enhances its transforming ability. *J Biol Chem.* 2011;286:38989–39001.
- Nikoletopoulou V, Markaki M, Palikaras K, Tavernarakis N. Crosstalk between apoptosis, necrosis and autophagy. *Biochim Biophys Acta.* 2013;1833:3448–3459.
- Meng H, Liu Z, Li X, et al. Death-domain dimerization-mediated activation of RIPK1 controls necroptosis and RIPK1-dependent apoptosis. *Proc Natl Acad Sci U S A.* 2018;115:E2001–E2009.
- Kong XN, Yan HX, Chen L, et al. LPS-induced down-regulation of signal regulatory protein {alpha} contributes to innate immune activation in macrophages. *J Exp Med.* 2007;204:2719–2731.

- 25 Walsh CJ, Hu P, Batt J, Santos CC. Microarray meta-analysis and cross-platform normalization: integrative genomics for robust biomarker discovery. *Microarrays (Basel)*. 2015;4:389–406.
- 26 Pan YF, Tan YX, Wang M, et al. Signal regulatory protein alpha is associated with tumor-polarized macrophages phenotype switch and plays a pivotal role in tumor progression. *Hepatology*. 2013;58:680–691.
- 27 Hara K, Senga T, Biswas MH, et al. Recovery of anoikis in Src-transformed cells and human breast carcinoma cells by restoration of the SIRP alpha1/SHP-2 signaling system. *Cancer Res*. 2011;71:1229–1234.
- 28 Peng L, Zhang H, Hao Y, et al. Reprogramming macrophage orientation by microRNA 146b targeting transcription factor IRF5. *EBioMedicine*. 2016;14:83–96.
- 29 Morris DL, Singer K, Lumeng CN. Adipose tissue macrophages: phenotypic plasticity and diversity in lean and obese states. *Curr Opin Clin Nutr Metab Care*. 2011;14:341–346.
- 30 Kim JK, Lee HM, Park KS, et al. MIR144* inhibits antimicrobial responses against Mycobacterium tuberculosis in human monocytes and macrophages by targeting the autophagy protein DRAM2. *Autophagy*. 2017;13:423–441.
- 31 Ouimet M, Koster S, Sakowski E, et al. Mycobacterium tuberculosis induces the miR-33 locus to reprogram autophagy and host lipid metabolism. *Nat Immunol*. 2016;17:677–686.
- 32 Pagan AJ, Yang CT, Cameron J, et al. Myeloid growth factors promote resistance to mycobacterial infection by curtailing granuloma necrosis through macrophage replenishment. *Cell Host Microbe*. 2015;18:15–26.
- 33 Matty MA, Roca FJ, Cronan MR, Tobin DM. Adventures within the speckled band: heterogeneity, angiogenesis, and balanced inflammation in the tuberculous granuloma. *Immunol Rev*. 2015;264:276–287.
- 34 Dey A, Mustafi SB, Saha S, Kumar Dhar Dwivedi S, Mukherjee P, Bhattacharya R. Inhibition of BMI1 induces autophagy-mediated necroptosis. *Autophagy*. 2016;12:659–670.
- 35 Geng W, Ng KT, Sun CK, et al. The role of proline rich tyrosine kinase 2 (Pyk2) on cisplatin resistance in hepatocellular carcinoma. *PLoS One*. 2011;6:e27362.
- 36 Okenwa C, Kumar A, Rego D, et al. SHP-1-Pyk2-Src protein complex and p38 MAPK pathways independently regulate IL-10 production in lipopolysaccharide-stimulated macrophages. *J Immunol*. 2013;191:2589–2603.
- 37 Diao Y, Ma X, Min W, et al. Dasatinib promotes paclitaxel-induced necroptosis in lung adenocarcinoma with phosphorylated caspase-8 by c-Src. *Cancer Lett*. 2016;379:12–23.
- 38 Li L, Chen W, Liang Y, et al. The Gbetagamma-Src signaling pathway regulates TNF-induced necroptosis via control of necrosome translocation. *Cell Res*. 2014;24:417–432.
- 39 Zhang T, Zhang Y, Cui M, et al. CaMKII is a RIP3 substrate mediating ischemia- and oxidative stress-induced myocardial necroptosis. *Nat Med*. 2016;22:175–182.
- 40 Kurenova E, Xu LH, Yang X, et al. Focal adhesion kinase suppresses apoptosis by binding to the death domain of receptor-interacting protein. *Mol Cell Biol*. 2004;24:4361–4371.
- 41 Behar SM, Divangahi M, Remold HG. Evasion of innate immunity by Mycobacterium tuberculosis: is death an exit strategy? *Nat Rev Microbiol*. 2010;8:668–674.
- 42 Jorgensen I, Rayamajhi M, Miao EA. Programmed cell death as a defence against infection. *Nat Rev Immunol*. 2017;17:151–164.
- 43 Stutz MD, Ojaimi S, Allison C, et al. Necroptotic signaling is primed in Mycobacterium tuberculosis-infected macrophages, but its pathophysiological consequence in disease is restricted. *Cell Death Differ*. 2018;25:951–965.